

Copyright © 1984, by the author(s).
All rights reserved.

Permission to make digital or hard copies of all or part of this work for personal or classroom use is granted without fee provided that copies are not made or distributed for profit or commercial advantage and that copies bear this notice and the full citation on the first page. To copy otherwise, to republish, to post on servers or to redistribute to lists, requires prior specific permission.

A DOUBLE-SCROLL CHAOTIC ATTRACTOR
FROM A THIRD ORDER RECIPROCAL CIRCUIT

by

T. Matsumoto, L. O. Chua, and M. Komuro

Memorandum No. UCB/ERL M84/73

31 August 1984

Title
page

A DOUBLE-SCROLL CHAOTIC ATTRACTOR
FROM A THIRD ORDER RECIPROCAL CIRCUIT

by

T. Matsumoto, L. O. Chua, and M. Komuro

Memorandum No. UCB/ERL M84/73

31 August 1984

ELECTRONICS RESEARCH LABORATORY
College of Engineering
University of California, Berkeley
94720

A DOUBLE-SCROLL CHAOTIC ATTRACTOR
FROM A THIRD ORDER RECIPROCAL CIRCUIT

by

T. Matsumoto, L. O. Chua, and M. Komuro

Memorandum No. UCB/ERL M84/73

31 August 1984

ELECTRONICS RESEARCH LABORATORY

College of Engineering
University of California, Berkeley
94720

A DOUBLE-SCROLL CHAOTIC ATTRACTOR
FROM A THIRD ORDER RECIPROCAL CIRCUIT

T. Matsumoto[†]
L.O. Chua^{††}
M. Komuro^{†††}

ABSTRACT A detailed analysis is given of the geometric structure of a chaotic attractor observed with an extremely simple autonomous electrical circuit. It is third order, reciprocal and has only one nonlinear element: a 3-segment piecewise-linear resistor. In addition to a sheet-like composition the attractor contains a "double-scroll" structure, i.e., two sheet-like objects are curled up together into spiral forms with infinitely many rotations. Lyapunov exponents and Lyapunov dimension are computed. The attractor has one positive, one zero and one negative Lyapunov exponent. Lyapunov dimension turns out to be a fractal between 2 and 3 which agrees with the structures observed. Power spectra of the three state variables and a 1-dimensional map are also given.

† Department of Electrical Engineering, Waseda University, Tokyo, 160, Japan

†† Department of Electrical Engineering and Computer Sciences, University of California, Berkeley, CA 94720.

††† Department of Mathematics, Tokyo Metropolitan University, Tokyo 158, Japan

Research partially supported by the Office of Naval Research Contract N00014-70-C-0572.

I. INTRODUCTION

This paper gives a detailed analysis of a chaotic attractor observed with an extremely simple autonomous electrical circuit which was reported earlier [1], [2]. The circuit is third order, reciprocal, and has only one nonlinear element, a 3-segment piecewise-linear resistor.

Consider the circuit of Figure 1(a) where the constitutive relation of the nonlinear resistor is given by Figure 1 (b). The dynamics is described by

$$\begin{aligned}
 C_1 \frac{dv_{C_1}}{dt} &= G(v_{C_2} - v_{C_1}) - g(v_{C_1}) \\
 C_2 \frac{dv_{C_2}}{dt} &= G(v_{C_1} - v_{C_2}) + i_L \\
 L \frac{di_L}{dt} &= -v_{C_2}
 \end{aligned} \tag{1.1}$$

where v_{C_1} , v_{C_2} and i_L denote voltage across C_1 , voltage across C_2 and current through L , respectively and $g(v_{C_1})$ is the piecewise-linear function in Fig. 1(b) (+):

$$\begin{aligned}
 g(v_{C_1}) &= m_0 v_{C_1} + \frac{1}{2} (m_1 - m_0) | v_{C_1} + B_p | \\
 &\quad + \frac{1}{2} (m_0 - m_1) | v_{C_1} - B_p |
 \end{aligned} \tag{1.2}$$

Figure 2 shows the chaotic attractor observed by solving (1.1) with

$$\begin{aligned}
 1/C_1 &= 9, \quad 1/C_2 = 1, \quad 1/L = 7, \quad G = 0.7, \quad m_0 = -0.5, \\
 m_1 &= -0.8, \quad B_p = 1.
 \end{aligned} \tag{1.3}$$

A typical trajectory in the attractor rotates around one of the two "holes", say the upper hole, in a counterclockwise direction. After each rotation the trajectory gets further from the "center" of the hole until a

(+) Our choice of a piecewise-linear function is for convenience in analysis and programming. As will be seen in Section II, the piecewise-linearity simplifies the analysis in a significant manner. Any continuous piecewise-linear function has an explicit formula which requires only absolute value functions [3].

certain time after which there are two possibilities: (i) the trajectory goes back to a position closer to the center of the hole and repeats a similar process, (ii) the trajectory does not go back to a point close to the center but descends downward (with respect to the v_{C_1} - axis)

in a spiral path and "lands" on the lower part of the attractor. The point it lands is close to the center of the lower hole and it starts rotating counterclockwise around the lower hole. After this, the behavior is similar to that in the upper part of the attractor except for the fact that it starts ascending after rotating around the lower hole several times. The number of rotations a trajectory makes around a hole before it starts descending or ascending is random: two to eight times have been observed.

The number of rotations it makes while it descends or ascends is also random. Detailed reasoning for such behaviors will be given in Section II.

Now, it is interesting to observe that there is a closed orbit (broken curve) outside the chaotic attractor. It is not a stable limit cycle, since one does not observe it by simply iterating the Runge-Kutta. Neither it is a repelling periodic orbit since one does not observe it by iterating the Runge-Kutta with negative time. It is, rather, a hyperbolic [4] periodic orbit : its Poincare map is stable in one direction while unstable in another direction. Newton iteration was used to find an initial point on this orbit via the "shooting method" [5, Chap. 17].

If the reader feels uncomfortable with the function g of Figure 1(b) in that it is not eventually passive [11] and there are initial conditions with which (1.1) diverges, he can simply replace Figure 1(b) with Figure 3. If $\hat{B}_p=3$, it has no effect on the attractor and on the hyperbolic periodic orbit, because $|v_{C_1}(t)| < 3$ for all $t \geq 0$ on the attractor and on the additional hyperbolic periodic orbit. The only difference is the/appearance of a large stable limit cycle (periodic attractor) as shown in Figure 4 ($\hat{B}_p = 3, m_2 = 5$), where (1.1) does not diverge with any initial condition.

In Fig. 4 there are three initial conditions:

- (i) $v_{C_1}(0) = 0.15264$
- $v_{C_2}(0) = -0.02281$

$$i_L(0) = 0.38127$$

for the chaotic attractor,

$$(ii) \quad v_{C_1}(0) = 2.532735$$

$$v_{C_2}(0) = 1.285458 \times 10^{-3}$$

$$i_L(0) = -3.367482$$

for the hyperbolic periodic orbit with period 3.54793, and

$$(iii) \quad v_{C_1}(0) = -3.08832$$

$$v_{C_2}(0) = -1.0423$$

$$i_L(0) = 6.93155$$

for the large periodic attractor with period 2.87.

The attractor appears to persist in a strong manner: the shape does not seem to change qualitatively with fairly large variations of parameters. It has been observed that the attractor persists for at least the following parameter ranges:

$$(i) \quad 8.82 \leq \frac{1}{C_1} \leq 10.6, \text{ when } \frac{1}{C_2} = 1, \frac{1}{L} = 7 \text{ and } G = 0.7 \text{ are fixed,}$$

$$(ii) \quad 0.5 \leq \frac{1}{C_2} \leq 1.08, \text{ when } \frac{1}{C_1} = 9, \frac{1}{L} = 7 \text{ and } G = 0.7 \text{ are fixed,}$$

$$(iii) \quad 5.7 \leq \frac{1}{L} \leq 7.13, \text{ when } \frac{1}{C_1} = 9, \frac{1}{C_2} = 1 \text{ and } G = 0.7 \text{ are fixed, and}$$

$$(iv) \quad 0.68 \leq G \leq 0.76, \text{ when } \frac{1}{C_1} = 9, \frac{1}{C_2} = 1 \text{ and } \frac{1}{L} = 7 \text{ are fixed.}$$

Since there are two attractors in Fig. 4 (the chaotic attractor and the periodic attractor), one naturally wonders what object separates the domain of attraction for the chaotic attractor and the domain of attraction for the periodic attractor. Similarly, in Fig. 2, one wonders what distinguishes those initial states that are attracted to the chaotic attractor and those initial states with which (1.1) diverges. This is an interesting but a hard question. It appears that the stable manifold of the hyperbolic periodic orbit decomposes R^3 into two regions

in a very complicated manner.

Observations so far are with digital computers. It is easy to realize (1.1) by a real circuit. Fig. 5 shows the attractor seen by an oscilloscope. Fig. 6(a) gives the circuitry where the subcircuit within the box realizes the function g of Fig. 1 (b) at least in the region where the attractor lies. The constitutive relation observed is given by Fig. 6(b). Saturation of the Op. Amp. naturally gives rise to eventual passivity for g . The saturation occurs, however, in regions away from the attractor and it does not affect the attractor.

The set of parameter values given by (1.3) is different from the one reported in [1]; namely,

$$1/C_1=10, 1/C_2=0.5, 1/L=7, G=0.7, m_0=-0.1, m_1=-4, B_p=1 \quad (1.4)$$

Equation for $g(v_{C_1})$ is given by (1.2).

The attractor observed with the set of parameter values in (1.4) is shown in Fig. 7. Of course, a large stable limit cycle is present in this case also if one replaces g of Fig. 1 (b) with Fig. 3 ($m_2=5, \hat{B}_p=14$). Let us explain why we chose (1.3) instead of (1.4). In Fig. 7, a typical trajectory in the attractor behaves in a manner similar to that of Fig. 2(a) except that the "spiral staircase" was not clearly visible and that the trajectories which go back closer to the center of the hole without descending were indiscernible. When Fig. 7 was first observed [1] a natural question was "What object separates those trajectories which remain in the upper ring and those which move down to the lower ring?" If that object was the structure detected, then an important part of /of the attractor would be understandable. We tried to find this "object" numerically by changing initial conditions. It was extremely sensitive to the initial conditions and we were unable to detect it. In order to see the reason note that the behavior of (1.1) is strongly influenced by the eigen values and eigen spaces of its equilibria,

since it is piecewise-linear and since each region has a unique equilibrium. Note that (1.1) has three equilibria: one at the origin, one located approximately at the center of the upper hole, call it p^+ , and another located at the point symmetric with respect to the origin, call it p^- . Each equilibrium has one real eigen value and two complex conjugate eigen values. At p^+ (and p^-) the real eigen value associated with (1.4) is

$$\gamma_p \approx -6.37$$

and the other two are

$$\alpha_p \pm j \beta_p \approx 0.01 \pm j 1.82$$

At the origin, the eigen values are

$$\gamma_o \approx 33.07$$

$$\alpha_o \pm j \beta_o \approx -0.21 \pm j 1.86$$

It is clear that γ_o , the real eigen value at the origin, completely overwhelms others, i.e., expansion at the origin is extremely strong and a digital computer (a finite discrete machine) is unable to show the structure of the continuous flow generated by (1.1) with (1.4).

With (1.3), the eigen values are

$$\gamma_p \approx -2.76$$

$$\alpha_p \pm j \beta_p \approx 0.13 \pm j 2.13$$

$$\gamma_o \approx 1.55$$

$$\alpha_o \pm j \beta_o \approx -0.68 \pm j 1.90$$

All of them are within a compatible range and the object that we were looking for turned out to be the stable eigenspace of the origin.

Moreover, an interesting structure different from Lorenz's [7] and Rössler's [8] has been observed as will be described in the next section.

Finally, note that the function g of Fig. 1 (b) does not have to be piecewise-linear to observe qualitatively the same attractor. Let us replace, for example, g of Fig. 1(b) with the smooth cubic function,

$$g(v_{C_1}) = a_0 v_{C_1} \left(\frac{a_1}{3} v_{C_1}^2 - 1 \right), \quad (1.5)$$

where $a_0 = 0.8$, $a_1 = 0.1$. Then with $1/C_1 = 9$, $1/C_2=2$, $1/L = 7$, $G = 0.65$, a chaotic attractor of Fig. 8 has been observed.

In section II we will give a detailed description of the geometric structure of the attractor. In Section III, we will give our computation of the Lyapunov exponents which give important quantitative information associated with an attractor, and then calculate the Lyapunov dimension. It turns out to be a fractal between 2 and 3. Finally, in Section IV, we will give the power spectra of the three state variables and a 1-dimensional map at a certain cross section.

II. GEOMETRIC STRUCTURE OF THE ATTRACTOR

2.1 Preliminary Observations

Recall the dynamics (1.1) and note that the function g of Fig. 1(b) is given by

$$g(v_R) \triangleq g(v_R; B_p, m_0, m_1)$$

$$= \begin{cases} m_0 v_R + B_p (m_1 - m_0) , & v_R \geq B_p \\ m_1 v_R & , |v_R| \leq B_p \\ m_0 v_R - B_p (m_1 - m_0) , & v_R \leq -B_p \end{cases} \quad (2.1)$$

This function satisfies

$$g(B_p v_R; B_p, m_0, m_1) = B_p g(v_R; 1, m_0, m_1) \quad (2.2)$$

Therefore, using the following normalized dimensionless variables and parameters

$$x \triangleq v_{C_1} / B_p, \quad y \triangleq v_{C_2} / B_p, \quad z \triangleq i_L / (B_p G), \quad \tau \triangleq tG / C_1, \quad (2.3)$$

$$n_0 \triangleq m_0 / G, \quad n_1 \triangleq m_1 / G, \quad S \triangleq C_2 / C_1, \quad T \triangleq C_2 / (LG^2),$$

equation (1.1) is transformed into

$$\boxed{\begin{aligned} \frac{dx}{d\tau} &= S(y - x - f(x)) \\ \frac{dy}{d\tau} &= x - y + z \\ \frac{dz}{d\tau} &= -Ty \end{aligned}} \quad (2.4)$$

where,

$$f(x) \triangleq g(x; 1, n_0, n_1)$$

$$= \begin{cases} n_0 x + n_1 - n_0, & x \geq 1 \\ n_1 x & , |x| \leq 1 \\ n_0 x - n_1 + n_0, & x \leq -1 \end{cases} \quad (2.5)$$

Equation (2.4) is dynamically equivalent to (1.1) but is more convenient since some of the parameters are normalized. Our analysis below will be based on (2.4). This form will also be convenient when we discuss various bifurcations in later papers.

We begin with the following observations:

- (i) Equation (2.4) is symmetric with respect to the origin, i.e. the vector field is invariant under the transformation

$$(x, y, z) \longrightarrow (-x, -y, -z). \quad (2.6)$$

- (ii) Consider the equilibria:

$$\begin{cases} x + f(x) = 0 \\ y = 0 \\ x + z = 0 \end{cases} \quad (2.7)$$

It follows from the form of f that (2.4) has a unique equilibrium in each of the following three subsets of \mathbb{R}^3 :

$$\begin{cases} D_1 \triangleq \{(x, y, z) \mid x \geq 1\} \\ D_0 \triangleq \{(x, y, z) \mid |x| \leq 1\} \\ D_{-1} \triangleq \{(x, y, z) \mid x \leq -1\} \end{cases} \quad (2.8)$$

provided that $n_0, n_1 \neq -1$. The equilibria are explicitly given by

$$\begin{cases} P^+ = (k, 0, -k) \in D_1 \\ Q = (0, 0, 0) \in D_0 \\ P^- = (-k, 0, k) \in D_{-1} \end{cases} \quad (2.9)$$

where $k = (n_0 - n_1)/(n_0 + 1)$

- (iii) In each of D_1, D_0 and D_{-1} , (2.4) is linear. In fact, letting

$$\underline{x} \triangleq (x, y, z), \quad \underline{k} \triangleq (k, 0, -k) \quad (2.10)$$

$$\underline{M}(S, T, n) \triangleq \begin{bmatrix} -S(n+1) & S & 0 \\ 1 & -1 & 1 \\ 0 & -T & 0 \end{bmatrix} \quad (2.11)$$

we can recast (2.4) as follows:

$$\frac{d\underline{x}}{dt} = \begin{cases} \underline{M}(S, T, n_0) (\underline{x} - \underline{k}), & \underline{x} \in D_1 \\ \underline{M}(S, T, n_1) \underline{x}, & \underline{x} \in D_0 \\ \underline{M}(S, T, n_0) (\underline{x} + \underline{k}), & \underline{x} \in D_{-1} \end{cases} \quad (2.12)$$

where we are abusing our notation for time: it should have been τ instead of t (see (2.3)). There will be no confusion, however. The set of parameter values (S, T, n_0, n_1) corresponding to (1.3) is given (via (2.3)) by

$$(S, T, n_0, n_1) = (9, 14\frac{2}{7}, -\frac{5}{7}, -\frac{8}{7}) \quad (2.13)$$

Then the matrix

$$\underline{M}_p \triangleq \underline{M}(9, 14\frac{2}{7}, -\frac{5}{7})$$

has real eigen value

$$\gamma_p \approx -3.94 \quad (2.14)$$

and a pair of complex conjugate eigen values

$$\alpha_p \pm j \beta_p \approx 0.19 \pm j 3.05 \quad (2.15)$$

Similarly, the matrix

$$\underline{M}_0 \triangleq \underline{M}(9, 14\frac{2}{7}, -\frac{8}{7})$$

has eigen values

$$\gamma_0 \approx 2.22 \quad (2.16)$$

$$\alpha_0 \pm j \beta_0 \approx -0.97 \pm j 2.71 \quad (2.17)$$

Note that the relative sizes of eigen values remain unchanged even after rescaling via (2.3). Let $E^s(\underline{p}^\pm)$ be the eigen space corresponding to the eigen value γ_p at \underline{p}^\pm and let $E^u(\underline{p}^\pm)$ be the eigen space[†]

[†]Throughout this paper, we use the same terminology "eigen space" to denote the vector space spanned by the real and imaginary parts of the complex conjugate eigen vectors.

corresponding to $\alpha_p \pm j \beta_p$ at P_p^\pm . Similarly, let $E^u(Q)$ and $E^s(Q)$ be the eigen spaces corresponding to γ_0 and $\alpha_0 \pm j \beta_0$, respectively. Then

$$\dim E^s(\tilde{P}_p^\pm) = \dim E^u(Q) = 1$$

$$\dim E^u(\tilde{P}_p^\pm) = \dim E^s(Q) = 2$$

and they are given explicitly by the following equations:

$$E^s(\tilde{P}_p^\pm) : \frac{x \mp k}{S\gamma_p} = \frac{y}{\gamma_p(\gamma_p + S(n_0 + 1))} = \frac{z \pm k}{-T(\gamma_p + S(n_0 + 1))}$$

$$E^u(\tilde{P}_p^\pm) : (\gamma_p^2 + \gamma_p + T)(x \mp k) + S\gamma_p y - S(z \pm k) = 0$$

$$E^u(Q) : \frac{x}{S\gamma_0} = \frac{y}{\gamma_0(\gamma_0 + S(n_1 + 1))} = \frac{z}{-T(\gamma_0 + S(n_1 + 1))}$$

$$E^s(Q) : (\gamma_0^2 + \gamma_0 + T)x + S\gamma_0 y - Sz = 0$$

2.2 The Geometric Structure

Now we turn to describe the structure of the attractor. Define

(see Fig. 9)

$$U_1 \triangleq D_1 \cap D_0 = \{ (x, y, z) \mid x = 1 \}$$

$$U_{-1} \triangleq D_{-1} \cap D_0 = \{ (x, y, z) \mid x = -1 \}$$

$$V \triangleq \{ (x, y, z) \mid \dot{x} = 0 \} = \{ (x, y, z) \mid y - x - f(x) = 0 \}$$

$$L_0 \triangleq E^u(\tilde{P}_p^+) \cap U_1$$

$$L_1 \triangleq E^s(Q) \cap U_1$$

$$L_2 \triangleq V \cap U_1$$

$$A \triangleq L_0 \cap L_1, \quad B \triangleq L_0 \cap L_2$$

$$C \triangleq E^u(Q) \cap U_1, \quad C^- \triangleq E^u(Q) \cap U_{-1}$$

$$D \triangleq E^s(P^+) \cap U_1, \quad D^- \triangleq E^s(P^-) \cap U_{-1}.$$

$F \triangleq$ a point on L_0 sufficiently far from B .

Note that U_1 , U_{-1} and V are 2-dimensional objects, L_0 , L_1 and L_2 are lines while A , B , C , C^- , D , D^- and F are points. Let φ^t be the flow generated by (2.4) and pick an initial condition $x_0 \in E^u(P^+)$ in a neighborhood of P^+ . Then, for $t > 0$, the flow $\varphi^t(x_0)$ starts wandering away from P^+ on $E^u(P^+)$. After winding round P^+ several times in a counterclockwise direction, it hits the plane U_1 at some time, say $t_1: x_1 \triangleq \varphi^{t_1}(x_0)$. The trajectory up to t_1 is a spiral since (2.4) is linear in D_1 and since $E^u(P^+)$ is invariant. Clearly $x_1 \in L_0$. Note that the line L_2 is a straight line parallel to the z -axis because \dot{x} is independent of z . Observe that L_2 separates the plane U_1 into two regions, one (to which A belongs) where $\dot{x} < 0$ and another where $\dot{x} > 0$. Since $\varphi^t(x_0)$ hits the plane U_1 downward (recall that the motion is counterclockwise) at $t = t_1$, one sees that x_1 belongs to the line segment \overline{FB} , i.e., $\dot{x} < 0$ at x_1 . The "fate" of $\varphi^t(x_1)$ depends crucially on which part of \overline{FB} x_1 lies. (see Fig. 10)

Case 1 $x_1 = A$

Numerical observations show that $\varphi^t(A)$ never hits U_{-1} . Since $A \in E^s(Q)$ and since $E^s(Q)$ is invariant, $\varphi^t(x_1)$ approaches the origin asymptotically as $t \rightarrow \infty$. The trajectory is a spiral with infinitely many rotations because (2.4) is linear in D_0 and $E^s(Q)$ is invariant.

Case 2 $x_1 \in \text{Interior } \overline{AB}$

In this case $\varphi^t(x_1)$ has two components: one which is in $E^s(Q)$ and approaches the origin asymptotically and another which stays on $\overline{QC} \subset E^u(Q)$ and wanders away from the origin. This means that $\varphi^t(x_1)$ moves up along a spiral with central axis \overline{QC} and then eventually hits U_1 again from

below: $\underline{x}_2 \triangleq \varphi^{t_2}(\underline{x}_1)$. The number of rotations of $\varphi^t(\underline{x}_1)$ around \overline{OC} can get arbitrarily large without bound if \underline{x}_1 is very close to A. These processes naturally give rise to the map

$$\underline{\Psi} : \overline{AB} \rightarrow U_1$$

defined by

$$\underline{\Psi}(\underline{x}_1) = \underline{x}_2$$

The image $\underline{\Psi}(\overline{AB})$ is a spiral with center at C which is tangent to L_0 at B. After hitting U_1 , the trajectory $\varphi^t(\underline{x}_2)$ has two components: one which stays in $E^u(\underline{P}^+)$ and moves away from \underline{P}^+ in a spiral manner and another in $E^s(\underline{P}^+)$ which approaches \underline{P}^+ asymptotically. Therefore $\varphi^t(\underline{x}_2)$ ascends in a spiral path with central axis \overline{DP}^+ and flattens itself onto $E^u(\underline{P}^+)$ from below.

Case 3 $\underline{x}_1 \in \text{Interior } \overline{FA}$

$\varphi^t(\underline{x}_1)$ has two components. One component stays in $E^s(Q)$ and asymptotically approaches Q in a spiral manner. Another component stays in $E^u(Q)$ and moves away from Q on \overline{OC}^- . This means that $\varphi^t(\underline{x}_1)$ descends along a spiral with central axis \overline{OC}^- , hits U_{-1} at $\underline{x}_2 \triangleq \varphi^{t_2}(\underline{x}_1)$ and enters the region D_{-1} eventually. The closer \underline{x}_1 to the point A, the larger the number of rotations of $\varphi^t(\underline{x}_1)$ around \overline{OC}^- . After entering into D_{-1} , the flow $\varphi^t(\underline{x}_2)$ consists of two components: one which is in $E^u(\underline{P}^-)$ and moves away from \underline{P}^- and another which stays in $E^s(\underline{P}^-)$ and asymptotically approaches \underline{P}^- . Therefore, $\varphi^t(\underline{x}_2)$ descends spirally with the central axis \overline{DP}^- and eventually flattens itself onto $E^u(\underline{P}^-)$ from above.

In order to grasp the whole picture, pick a rectangle $abcd$ in D_1 in such a way that \overline{ad} is on $E^u(\underline{P}^+)$ and \overline{bc} lies below $E^u(\underline{P}^+)$, i.e., on the side to which D belongs. Fig. 11 shows how the rectangle $abcd$ changes its shape while flowing along φ^t . Suppose that the rectangle is thin enough and that it is chosen appropriately in such a way that the trajectories starting on the line segment \overline{ef} hit L_1 . Then, after

hitting L_0 , they approach the origin asymptotically in a spiral manner with infinitely many rotations. Trajectories starting in the rectangle $abfe$ stay within D_1 or return to D_1 eventually even if they once spend sometime in D_0 . Trajectories with initial states in the rectangle $cdef$ leave D_1 , enter D_0 , hit U_{-1} and enter D_{-1} . They turn round \underline{P}^- and flatten themselves onto $E^u(\underline{P}^-)$ from above. Since (2.4) is symmetric with respect to the origin, one sees that a similar argument applies to a rectangle $\bar{a}\bar{b}\bar{c}\bar{d}$ in region U_{-1} located symmetrically with respect to the origin. Assembling all the information, one obtains a whole picture (Fig. 12). Observe that the rectangle $abcd$ is mapped into two spiral regions with infinitely many rotations: $abfe$ is mapped into one spiral region and $cdef$ into another spiral region. Note that $E^S(Q)$ plays an important role in determining the fate of a trajectory after hitting U_1 or U_{-1} . It differentiates those trajectories which descend (resp. ascend) from those which survive in the upper part (resp. lower part). This is barely discernible in Fig. 2(a) if one takes a careful look at it. There are two thin gaps between the sets of trajectories and $E^S(Q)$ is sitting in these gaps.

Finally, let us explain why one observes a sheet-like structure in the attractor. First let $\underline{\Phi}(t)$ be the fundamental matrix solution to the variational equation of (2.4) along a trajectory $\underline{\varphi}^t(\underline{x}_0)$. Then its determinant $\det \underline{\Phi}(t)$ satisfies [6]

$$\frac{d}{dt} (\det \underline{\Phi}(t)) = \text{divergence} \left(\frac{d}{dt} \underline{\varphi}^t(\underline{x}_0) \right) (\det \underline{\Phi}(t))$$

and it gives the linearized contraction or expansion rate of volume elements along a trajectory $\underline{\varphi}^t(\underline{x}_0)$. In D_1 and D_{-1} ,

$$\text{divergence} \left(\frac{d}{dt} \underline{\varphi}^t(\underline{x}_0) \right) = \text{trace } \underline{M}_p = -\frac{25}{7}$$

and in D_0 ,

$$\text{divergence} \left(\frac{d}{dt} \underline{\varphi}^t(\underline{x}_0) \right) = \text{trace } \underline{M}_0 = \frac{2}{7}.$$

It follows that volume elements are sharply contracted in D_1 and D_{-1} .

Even though volume elements are expanded in D_0 , the rate of expansion is very mild (2/7) and as a whole, volume elements are contracted.

This naturally gives rise to a "sheet-like" structure. Perhaps, a good way of explaining the whole picture described above would be the "double-scroll" structure since two sheet-like objects are curled up together into spiral forms with infinitely many rotations-while maintaining some space between the two scrolls which gradually decreases, thus causing them to meet eventually at some limit point. In order to see the structure more clearly let us look at the cross sections of the attractor.

Fig. 13 (b) - (k) show cross sections of the attractor taken at

$$U(r) \triangleq \{ (x, y, z) \mid x = r \}$$

$$r = 0.25 k, \quad k = 0, 1, \dots, 8$$

and at $U(2.20)$. (The cross section at $U(2.25)$ is extremely small.)

Fig. 13 (a) shows positions of the cross sections. On the cross section at $U(1.00)$, various line segments and points related to Fig. 9 - Fig. 12 are super imposed. One can clearly observe the double-scroll structure and how the scrolls flatten themselves gradually. The cross section at $U(1.75)$ (Fig. 13(i)) is particularly interesting. The sheet-like structure is clearly discernible : it is folded many times. Moreover, one can observe that the flattening of the left portion is sharper than that of the right portion so that the spirals still survive on the right portion while they flatten themselves on the left portion. This stems from the fact that trajectories rotate around \underline{P}^+ counterclockwise and hence they flatten onto $E^u(\underline{P}^+)$ as time goes. Note that theoretically, the two scrolls are curled up infinitely many times even though numerical results reveal only several of them. One can also observe how $E^s(Q)$ cuts the attractor. In Fig. 13 (b), (c) and (d), there are small gaps in the spirals. Since $E^s(Q)$ is sitting in the gaps, the trajectories cannot

get there (as long as numerical computations go). Those gaps correspond to the gaps in Fig. 2(a) as explained earlier. Fig. 14 is our final picture showing the structure of our attractor after several simplifications.

Now it is clear that the attractor reported in this paper has a structure different from Lorenz's [7] and Rössler's [8] since the double-scroll structure has not been observed with the latter attractors. Recall that the Lorenz equation (at the popular parameter values $\sigma = 10$, $\beta = 8/3$, $\rho = 28$) has three equilibria : one at the origin, one in the half space $x > 0$ and another in the half space $x < 0$. Note that the origin belongs to the Lorenz attractor and that ^{the} same is true for our attractor. The origin for the Lorenz attractor, however, is a saddle, i.e., all eigen values are real, whereas in our case the origin has one positive real eigen value and a pair of complex conjugate eigen values. Recall also that the Lorenz equation is symmetric with respect to the z-axis while (1.1) is symmetric with respect to the origin. As for the Rössler equation [8], recall that it has only two equilibria. Furthermore, the attractor does not contain any equilibrium.

One of the reviewers for [1] pointed out that Sparrow [9] and Brockett [10] had observed chaotic attractors in feedback systems with 3-segment piecewise-linear feedback characteristics. Their equations also have three equilibria. The one reported in [9] does not appear to have the double-scroll structure. It does not seem to contain any equilibrium. Furthermore, the equilibrium in the middle has one negative real eigen value and a pair of complex conjugate eigen values with positive real part, which is different from ours.

The dynamics reported in [10] has the same type of equilibria as ours. It is not clear if it has the double-scroll structure described above. In order to see a possible difference, recall the set D_1 defined by (2.8).

A trajectory with initial condition in D_1 (and in the attractor) first rotates around \underline{p}^+ several times before hitting D_0 . We have observed, however, by simulation, that with the dynamics reported in [10], a trajectory with initial condition in the region corresponding to D_1 seems to always penetrate U_1 while winding around the equilibrium corresponding to \underline{p}^+ .

Note also that the circuit of Fig. 1 has no coupling elements and hence reciprocal [11], while the systems in [7]-[10] do not appear to be realizable by reciprocal circuits.

III. LYAPUNOV EXPONENTS AND LYAPUNOV DIMENSION

3.1 Lyapunov Exponents

First let us write (1.1) as

$$\frac{dx}{dt} = \tilde{F}(x) \quad (3.1)$$

where $x = (v_{C_1}, v_{C_2}, i_L)$ and let $\varphi^t(x_0)$ be its flow with initial condition x_0 . (We are abusing the notation x . There will be no confusion, however.)

Lyapunov exponents are a generalization of characteristic exponents for periodic orbits to more general non-periodic orbits. If Λ is a periodic orbit with period T and if $x_0 \in \Lambda$, then the eigen values of $(D\varphi^T)_{x_0}$, denoted by e^{λ_1} , e^{λ_2} and e^{λ_3} , are called the characteristic multipliers for Λ . The numbers $\ln e^{\lambda_1}$, $\ln e^{\lambda_2}$ and $\ln e^{\lambda_3}$ are called the characteristic exponents.[†]

They give the expansion and the contraction rates of vectors in the tangent space $T_{x_0} R^3$ along Λ . Since Λ is a closed curve, at least one of the three numbers, say e^{λ_1} , must be 1, and hence $\ln e^{\lambda_1} = 0$. If, in addition, $\ln e^{\lambda_2}, \ln e^{\lambda_3} < 0$, then Λ will be a periodic attractor, i.e., a stable limit cycle (Fig. 15(a)). If $\ln e^{\lambda_2} < 0$ and $\ln e^{\lambda_3} > 0$, then Λ will be a hyperbolic periodic orbit (Fig. 15(b)). Now let Λ be a non-periodic invariant set, e.g., a chaotic attractor. There is a difficulty in defining characteristic multipliers for Λ . Recall that for a closed orbit, the eigen values of $(D\varphi^T)_{x_0}$ are well defined since $(D\varphi^T)_{x_0}$ maps $T_{x_0} R^3$ into itself. On the other hand, such argument is not valid for Λ if it is non-periodic since $(D\varphi^t)_{x_0}$ does not necessarily map $T_{x_0} R^3$ into itself for any t .

The definition of Lyapunov exponents requires the invariance of tangent subbundles. Suppose that for all $t > 0$, there are linear subspaces $E^1_{\varphi^t(x_0)} \supseteq E^2_{\varphi^t(x_0)} \supseteq E^3_{\varphi^t(x_0)}$ in $T_{\varphi^t(x_0)} R^3$ and numbers $\mu_1(x_0) \geq \mu_2(x_0) \geq \mu_3(x_0)$

[†] Of course, $\ln e^{\lambda_k} = \lambda_k$ for the periodic case. The above choice is meant to draw the analogy with the Lyapunov exponents for non-periodic case where the natural log is traditionally used.

such that

$$(i) \quad (D\varphi^t)_{\underline{x}_0} E_{\underline{x}_0}^k = E_{\varphi^t(\underline{x}_0)}^k \quad (3.2)$$

$$(ii) \quad \dim E_{\varphi^t(\underline{x}_0)}^k = 4 - k \quad (3.3)$$

$$(iii) \quad \mu_k(\underline{x}_0) = \lim_{T \rightarrow \infty} \frac{1}{T} \ln \frac{\| (D\varphi^T)_{\underline{x}_0} \underline{e} \|}{\| \underline{e} \|}$$

$$\text{for all } \underline{e} \in E_{\underline{x}_0}^k - E_{\underline{x}_0}^{k+1},$$

$$k = 1, 2, 3.$$

The numbers $\mu_1(\underline{x}_0)$, $\mu_2(\underline{x}_0)$ and $\mu_3(\underline{x}_0)$ are called the Lyapunov exponents for Λ if $\underline{x}_0 \in \Lambda$. They give the average linearized expansion and contraction rates on an orbit. Note that $E_{\underline{x}_0}^1 - E_{\underline{x}_0}^2$ consists of vectors in $T_{\underline{x}_0} \mathbb{R}^3$ which expand at the fastest rate, $E_{\underline{x}_0}^2 - E_{\underline{x}_0}^3$ consists of vectors which expand at the next fastest rate and the vectors in $E_{\underline{x}_0}^3$ expand at the slowest rate. In many cases the vectors in $E_{\underline{x}_0}^3$ are contracted if Λ is an attractor.

The conditions under which Lyapunov exponents exist are strong [12] and are hard to check. Here we will only give our numerical results. They give, however, good quantitative information about the attractor described in the previous sections. The computations are non trivial since one does not know the invariant splitting $E_{\varphi^t(\underline{x}_0)}^k$, $k = 1, 2, 3$. One can, however, compute $\mu_1(\underline{x}_0)$, the largest exponent, numerically provided that $\mu_1(\underline{x}_0)$, $\mu_2(\underline{x}_0)$ and $\mu_3(\underline{x}_0)$ are not too close to each other. In order to explain this, let $\underline{x}_0 \in \Lambda$ and pick any $\underline{e} \in T_{\underline{x}_0} \mathbb{R}^3$.

Then

$$\frac{1}{T} \ln \frac{\| (D\varphi^T)_{\underline{x}_0} \underline{e} \|}{\| \underline{e} \|} \quad (3.4)$$

would give $\mu_1(\underline{x}_0)$ for T large, because the subspace with the fastest expansion rate would eventually dominate others and the vector $(D\varphi^t)_{\underline{x}_0} \underline{e}$

would be in $E^1_{\underline{\varrho}^T(\underline{x}_0)} - E^2_{\underline{\varrho}^T(\underline{x}_0)}$ for any $\underline{e} \in T_{\underline{x}_0} \mathbb{R}^3$, T large.

Computations of $\mu_2(\underline{x}_0)$ and $\mu_3(\underline{x}_0)$ need some more care since $(D\underline{\varrho}^T)_{\underline{x}_0} \underline{e}$ is dominated by $E^1_{\underline{\varrho}^T(\underline{x}_0)} - E^2_{\underline{\varrho}^T(\underline{x}_0)}$ and one does not know how to compute $E^2_{\underline{\varrho}^T(\underline{x}_0)} - E^3_{\underline{\varrho}^T(\underline{x}_0)}$. In order to overcome this, one computes

$$\mu_1(\underline{x}_0) + \mu_2(\underline{x}_0) \tag{3.5}$$

instead of $\mu_2(\underline{x}_0)$. First note that the number (3.5) gives the average expansion or contraction rate of an area element of $E^1_{\underline{x}_0} - E^3_{\underline{x}_0}$. Let \underline{e}_1 and \underline{e}_2 span $E^1_{\underline{x}_0} - E^3_{\underline{x}_0}$. Then the exterior product $\underline{e}_1 \wedge \underline{e}_2$ is the parallelepiped generated by \underline{e}_1 and \underline{e}_2 [13]. Therefore,

$$\frac{1}{T} \ln \frac{\| (D\underline{\varrho}^T)_{\underline{x}_0} \underline{e}_1 \wedge (D\underline{\varrho}^T)_{\underline{x}_0} \underline{e}_2 \|}{\| \underline{e}_1 \wedge \underline{e}_2 \|} \tag{3.6}$$

would give (3.5) for T large. A numerical difficulty arises since $(D\underline{\varrho}^T)_{\underline{x}_0} \underline{e}_1$ and $(D\underline{\varrho}^T)_{\underline{x}_0} \underline{e}_2$ would eventually belong to or/very close to $E^1_{\underline{\varrho}^T(\underline{x}_0)} - E^2_{\underline{\varrho}^T(\underline{x}_0)}$ for the reason explained before. Hence the angle between $(D\underline{\varrho}^T)_{\underline{x}_0} \underline{e}_1$ and $(D\underline{\varrho}^T)_{\underline{x}_0} \underline{e}_2$ gets smaller and smaller, and numerical inaccuracy will be serious. In order to overcome this difficulty, recall that the map :

$$(\underline{e}_1, \underline{e}_2) \longrightarrow \underline{e}_1 \wedge \underline{e}_2$$

is bilinear, i.e., linear in each argument, and rewrite (3.6) as

$$\frac{1}{T} \ln \frac{\| [(D\underline{\varrho}^T)_{\underline{x}_0} \wedge (D\underline{\varrho}^T)_{\underline{x}_0}] (\underline{e}_1 \wedge \underline{e}_2) \|}{\| \underline{e}_1 \wedge \underline{e}_2 \|} \tag{3.7}$$

where

$$(D\underline{\varrho}^T)_{\underline{x}_0} \wedge (D\underline{\varrho}^T)_{\underline{x}_0} \tag{3.8}$$

is the induced linear map [13]. Since this is a 3×3 matrix and since

$$e_{12} \triangleq e_1 \wedge e_2 \tag{3.9}$$

is a 3-dimensional vector, one can compute (3.5) without the above difficulty.

The initial vector e_{12} of (3.9) can be chosen arbitrarily for the same

reason as e of (3.4) can be chosen arbitrarily, provided that

$\mu_1(x_0) + \mu_2(x_2)$ dominates $\mu_1(x_0) + \mu_3(x_0)$ and $\mu_2(x_0) + \mu_3(x_0)$ by

reasonable margins.

Finally, there is also a difficulty in computing $\mu_3(x_0)$ alone

for the same reason as before. One computes, instead,

$$\mu_1(x_0) + \mu_2(x_0) + \mu_3(x_0) \tag{3.10}$$

which gives the average contraction or expansion rate of a volume element

in $E_{x_0}^1$ assuming that $E_{x_0}^1 = T_{x_0} R^3$. An argument similar to the above

shows that

$$\frac{1}{T} \ln \frac{|| [(D\psi^T)_{x_0} \wedge (D\psi^T)_{x_0} \wedge (D\psi^T)_{x_0}] (e_1 \wedge e_2 \wedge e_3) ||}{|| e_1 \wedge e_2 \wedge e_3 ||} \tag{3.11}$$

would eventually give (3.10), where

$$\text{span} \{ e_1, e_2, e_3 \} = E_{x_0}^1 = T_{x_0} R^3$$

3.2 Computations

Based on the above arguments, we computed ^{the} Lyapunov exponent

$\mu_1(x_0)$ by solving the variational equation

$$\frac{dy}{dt} = (DF)_{\psi^t(x_0)} y \tag{3.12}$$

with

$$y(0) = e, \quad || e || = 1,$$

and computing

$$\frac{1}{T} \ln || \underline{y}(T) || \quad (3.13)$$

Our computation gives

$$\mu_1(\underline{x}_0) \approx 0.23 \quad (3.14)$$

where

$$\begin{cases} \underline{x}_0 = (-1.7713, 0.0527854, 1.74606) \\ \underline{e} = \left(\frac{1}{\sqrt{3}}, \frac{1}{\sqrt{3}}, \frac{1}{\sqrt{3}} \right) \\ T = 3000 \end{cases} \quad (3.15)$$

Of course, one has to renormalize $\underline{y}(t)$ after each reasonable amount of time since $||\underline{y}(t)||$ gets very large. More specifically, letting $T = n\tau$, one sees that

$$\begin{aligned} \frac{1}{T} \ln(||\underline{y}(T)||/||\underline{y}(0)||) &= \frac{1}{n\tau} \ln(||(\underline{D}\underline{\varphi}^{n\tau})_{\underline{x}_0} \underline{y}(0)||/||\underline{y}(0)||) \\ &= \frac{1}{n\tau} \ln(||(\underline{D}\underline{\varphi}^\tau)_{\underline{x}((n-1)\tau)} \underline{y}((n-1)\tau)||/||\underline{y}(0)||) \\ &= \frac{1}{n\tau} \ln \left(\frac{||(\underline{D}\underline{\varphi}^\tau)_{\underline{x}((n-1)\tau)} \underline{y}((n-1)\tau)||}{||(\underline{D}\underline{\varphi}^\tau)_{\underline{x}((n-2)\tau)} \underline{y}((n-2)\tau)||} \right. \\ &\quad \times \frac{||(\underline{D}\underline{\varphi}^\tau)_{\underline{x}((n-2)\tau)} \underline{y}((n-2)\tau)||}{||(\underline{D}\underline{\varphi}^\tau)_{\underline{x}((n-3)\tau)} \underline{y}((n-3)\tau)||} \\ &\quad \cdot \dots \\ &\quad \cdot \frac{||(\underline{D}\underline{\varphi}^\tau)_{\underline{x}_0} \underline{y}(0)||}{||\underline{y}(0)||} \left. \right) \\ &= \frac{1}{n\tau} \sum_{k=0}^{n-1} \ln \frac{||(\underline{D}\underline{\varphi}^\tau)_{\underline{x}(k\tau)} \underline{y}(k\tau)||}{||\underline{y}(k\tau)||} \quad (3.16) \end{aligned}$$

If one renormalizes

$$|| \underline{y}(k\tau) || = 1$$

at each k , then

$$\frac{1}{T} \ln || \underline{y}(T) || = \frac{1}{n\tau} \sum_{k=0}^{n-1} \ln || (D\underline{\varphi}^T)_{\underline{x}(k\tau)} \underline{y}(k\tau) || \quad (3.17)$$

In our case, we chose $\tau = 10$ with the Runge-Kutta step size 0.005.

Our experience indicates that (3.14) is insensitive to the initial tangent vector \underline{e} and to the initial condition \underline{x}_0 . The time $T = 3000$ seems to be enough for the convergence.

In order to compute (3.7) let

$$\underline{y} \triangleq (D\underline{\varphi}^t)_{\underline{x}_0} \underline{e}_1, \quad \underline{z} \triangleq (D\underline{\varphi}^t)_{\underline{x}_0} \underline{e}_2.$$

Then

$$\begin{aligned} \frac{d}{dt} (\underline{y} \wedge \underline{z}) &= \frac{d\underline{y}}{dt} \wedge \underline{z} + \underline{y} \wedge \frac{d\underline{z}}{dt} \\ &= [(D\underline{F})_{\underline{\varphi}^t(\underline{x}_0)} \underline{y}] \wedge \underline{z} + \underline{y} \wedge [(D\underline{F})_{\underline{\varphi}^t(\underline{x}_0)} \underline{z}] \\ &= [(D\underline{F})_{\underline{\varphi}^t(\underline{x}_0)} \wedge \underline{1} + \underline{1} \wedge (D\underline{F})_{\underline{\varphi}^t(\underline{x}_0)}] \underline{y} \wedge \underline{z} \end{aligned} \quad (3.18)$$

where $\underline{1}$ is the 3×3 identity matrix. (An explicit formula is given in the APPENDIX). Therefore, solving the "2-dimensional" variational equation (3.18) with

$$|| (\underline{y} \wedge \underline{z})(0) || = || \underline{e}_{12} || = 1$$

one can compute

$$\frac{1}{T} \ln || (\underline{y} \wedge \underline{z})(T) || .$$

Our computation gives

$$\mu_1(\underline{x}_0) + \mu_2(\underline{x}_0) \approx 0.23 \quad (3.19)$$

where \underline{x}_0 and T are the same as before and

$$\underline{e}_{12} = \left(\frac{1}{\sqrt{3}}, \frac{1}{\sqrt{3}}, \frac{1}{\sqrt{3}} \right).$$

Again (3.19) appears to depend neither on \underline{x}_0 nor \underline{e}_{12} .

Finally, observing that

$$(\underline{D}\underline{\varphi}^t)_{\underline{x}_0} \wedge (\underline{D}\underline{\varphi}^t)_{\underline{x}_0} \wedge (\underline{D}\underline{\varphi}^t)_{\underline{x}_0} = \det (\underline{D}\underline{\varphi}^t)_{\underline{x}_0} \quad (3.20)$$

and

$$\frac{d}{dt} \det (\underline{D}\underline{\varphi}^t)_{\underline{x}_0} = \text{trace } (\underline{DF})_{\underline{\varphi}^t(\underline{x}_0)} \det (\underline{D}\underline{\varphi}^t)_{\underline{x}_0} \quad (3.21)$$

one can compute (3.11). Our computation with the same \underline{x}_0 and T gives

$$\mu_1 (\underline{x}_0) + \mu_2 (\underline{x}_0) + \mu_3 (\underline{x}_0) \approx -0.05 \quad (3.22)$$

The convergence, however, seems to be very slow. At T = 3000 it is still increasing in an extremely slow manner. Further computations would not be very meaningful for numerical reasons. It is enough for our present purpose.

It follows from (3.14), (3.19) and (3.22) that

$$\begin{cases} \mu_1 (\underline{x}_0) \approx 0.23 \\ \mu_2 (\underline{x}_0) \approx 0 \\ \mu_3 (\underline{x}_0) \approx -0.28 \end{cases} \quad (3.23)$$

This shows that in the attractor observed, certain line elements are expanded, area elements are preserved and volume elements are contracted. This agrees with the sheet-like structure described in Section II. It would be interesting to compare (3.23) with those of Lorenz attractor. Even though the parameter values in [14] are different ($\sigma = 16$, $\beta = 4$, $\rho = 40$) from the popular ones, for they are enough/our present purpose:

$$\begin{cases} \mu_1 (\underline{x}_0) \approx 1.37 \\ \mu_2 (\underline{x}_0) \approx 0 \\ \mu_3 (\underline{x}_0) \approx -22.37 \end{cases} \quad (3.24)$$

The Lorenz attractor has much sharper expansion and contraction rates than the attractor reported in this paper. Note also that in the Lorenz attractor, volume elements are contracted uniformly since divergence = const. = -21.

3.3 Lyapunov Dimension

Dimension of a chaotic attractor is one of the very few quantitative measures which are associated with chaotic attractors. Among the many different definitions of dimension of chaotic attractors [15] we compute the Lyapunov dimension since it naturally comes from Lyapunov exponents. We are not saying that this is the most appropriate one. Recall (3.23) and recall that our numerical results indicate that these numbers do not seem to depend on x_0 . Assume that this is, in fact, the case. Then, since $\mu_1, \mu_1 + \mu_2 > 0$ and since $\mu_1 + \mu_2 + \mu_3 < 0$, Lyapunov dimension is given by [15]

$$d_L = 2 + \frac{\mu_1 + \mu_2}{|\mu_3|} \approx 2.82 \quad (3.25)$$

Let us compare this with the Lorenz attractor. It follows from (3.24) that for the Lorenz attractor,

$$d_L = 2 + \frac{1.37}{22.37} \approx 2.06 \quad (3.26)$$

Both of them are fractals between 2 and 3 which agree with the sheet-like structure observed. While d_L of our attractor is close to 3, d_L of the Lorenz attractor is close to 2. In this sense, our attractor is "thicker" than the Lorenz attractor (with $\sigma = 16, \beta = 4, \rho = 40$).

IV. POWER SPECTRA AND 1-DIMENSIONAL MAP

4.1 Power Spectra

Figure 16 shows the power spectra for the three state variables. In each case $N = 2^{16}$ Runge-Kutta iterations were performed with a step size equal to 0.04. (+) The figures show the components of the first $M=N/2^4=2^{12}$ normalized frequencies in log-log scale. The vertical scale is 10 dB/division. In each case, there is a sharp peak at $f = 828$. One has $\frac{N}{828} \times 0.04 \approx 3.166$ and this corresponds to the time a typical trajectory takes in rotating around P^+ or P^- . Power spectra for v_{C_1} and i_L have notable lower frequency components while power spectrum for v_{C_2} does not have such lower frequency components. This stems from the fact that the v_{C_2} -component of P^+ and P^- is zero while the v_{C_1} -component and the i_L -component are nonzero, and therefore, the oscillations of v_{C_2} have essentially no bias while oscillations of v_{C_1} and i_L are biased. The peak in the lower frequency components is at $f = 48$ which corresponds to the fact that the trajectory has gone "up and down" for 48 times, i.e., it has traversed the process $D_1 \rightarrow D_0 \rightarrow D_{-1}$ (see Section II) for 48 times and $D_{-1} \rightarrow D_0 \rightarrow D_1$ for another 48 times.

Figure 17 shows power spectra for v_{C_1} and v_{C_2} observed with the circuit of Fig. 6.

Finally, Fig. 18 shows a 1-dimensional map for i_L observed at the cross section $v_{C_1} = -1.6$, i.e., it consists of the plots of $i_L(t_n)$ versus $i_L(t_{n+1})$, where t_n is the n -th time for which $v_{C_1}(t)$ hits the plane $v_{C_1} = -1.6$ from below. Details of such 1-dimensional maps will be reported in a later paper.

(+) It is well known that FFT is very efficient if the number of samples is a power of 2.

APPENDIX

Here we will give an explicit formula for (3.18). Let $\{e_1, e_2, e_3\}$ be the standard basis for \mathbb{R}^3 . Then $e_1 \wedge e_2 = e_{12}$, $e_2 \wedge e_3 = e_{23}$, $e_1 \wedge e_3 = e_{13}$ are the standard basis for $(\mathbb{R}^3)^*$, the set of all alternating bilinear functions on $\mathbb{R}^3 \times \mathbb{R}^3$ [13] where \wedge denotes the exterior product. They satisfy,

$$e_i \wedge e_j = - e_j \wedge e_i, e_i \wedge e_i = 0.$$

Since (see (1.1))

$$(DF)_x = \begin{pmatrix} -\frac{1}{C_1} (G + (Dg)_{v_{C_1}}) & \frac{1}{C_1} G & 0 \\ \frac{1}{C_2} G & -\frac{1}{C_2} G & \frac{1}{C_2} \\ 0 & -\frac{1}{L} & 0 \end{pmatrix}$$

one can easily compute

$$(DF)_x \wedge \underline{1} = \begin{pmatrix} -\frac{1}{C_1} (G + (Dg)_{v_{C_1}}) & 0 & 0 \\ 0 & -\frac{1}{C_2} G & \frac{1}{C_2} G \\ 0 & \frac{1}{C_1} G & -\frac{1}{C_1} (G + (Dg)_{v_{C_1}}) \end{pmatrix}$$

$$\underline{1} \wedge (DF)_x = \begin{pmatrix} -\frac{1}{C_2} G & 0 & \frac{1}{C_2} \\ 0 & 0 & 0 \\ -\frac{1}{L} & 0 & 0 \end{pmatrix}$$

Therefore

$$(DF)_x \wedge \underline{1} + \underline{1} \wedge (DF)_x = \begin{pmatrix} - (G(\frac{1}{C_1} + \frac{1}{C_2}) + \frac{1}{C_1} (Dg)_{v_{C_1}}) & 0 & \frac{1}{C_2} \\ 0 & -\frac{1}{C_2} G & \frac{1}{C_2} G \\ -\frac{1}{L} & \frac{1}{C_1} G & -\frac{1}{C_1} (G + (Dg)_{v_{C_1}}) \end{pmatrix}$$

Remark Theoretically, there is a difficulty in using (3.12), (3.18) and (3.21) because g is piecewise-linear and Dg has discontinuities at $v_{C_1} = \pm 1$. Numerically, however, there seem to be no problem if one chooses a small enough Rung-Kutta step size.

References

- [1] T. Matsumoto, "A chaotic attractor from Chua's circuit", IEEE Trans. CAS, vol. CAS-32, 1985, in press.
- [2] G-Q Zhong and F. Ayrom, "Experimental confirmation of chaos from Chua's circuit", Int. J. Circuit Theory and Applications, vol. 13, Jan. 1985, in press.
- [3] L. O. Chua and S. M. Kang, "Section-wise piecewise-linear functions: canonical representation, properties, and applications", Proceedings of IEEE, vol. 65, No.6, pp. 915-929, 1977.
- [4] J. Guckenheimer and P. Holmes, Nonlinear Oscillations, Dynamical Systems, and Bifurcations of Vector Fields, Springer, New York, 1983.
- [5] L. O. Chua and P. M. Lin, Computer Aided Analysis of Electronic Circuits: Algorithms and Computational Techniques, Prentice-Hall, Englewood Cliffs, N. J., 1975 (Section 17.5).
- [6] M.W. Hirsch and S. Smale, Differential Equations, Dynamical Systems, and Linear Algebra, Academic Press, New York, 1974.
- [7] E. Lorenz, "Deterministic non-periodic flows", J. Atmosphere Science, vol. 20, pp 130-141, 1963.
- [8] O. Rössler, "An equation for continuous chaos", Phys. Lett., vol. 57A, pp 397-398, 1976.

- [9] C.T. Sparrow, "Chaos in a three dimensional single loop feed back system with a piecewise linear feedback function", J. Math. Anal. Appl. vol. 83, pp. 275 - 291, 1981.
- [10] R.W. Brockett, "On conditions leading to chaos in feedback systems", Proc. 1982 Conf. on D.C., IEEE, New York 1982.
- [11] L. O. Chua, "Dynamic nonlinear networks: state of the art", IEEE Trans. CAS, vol. CAS-27, pp 1059 - 1087, 1980.
- [12] V. I. Oseledec, "A multiplicative ergodic theorem : Lyapunov characteristic numbers for dynamical systems", Trans. Moscow Math. Soc., vol. 19, pp 197 - 231, 1968.
- [13] W. H. Fleming, Functions of Several Variables, Addison-Wesley, Reading, MA, 1965.
- [14] I. Shimada and T. Nagashima, "A numerical approach to ergodic problem of dissipative dynamical systems", Prog. Theor. Phys., vol. 61, pp 1605 - 1616, 1979.
- [15] L. S. Young, "Entropy, Lyapunov exponents and Hausdorff dimension in differentiable dynamical systems", IEEE Trans. CAS, vol. CAS-30, pp 599 - 607, 1983.

Acknowledgement During the course of this work, the authors have had exciting discussions with their friends, G. Ikegami of Nagoya University, S. Ichiraku of Yokohama City University, M. Ochiai of Shohoku Institute of Technology, Y. Togawa of Science University of Tokyo, K. Sawata of Toyohashi University of Technology and Science, S. Tanaka, T. Ando, H. Tomonaga, R. Tokunaga and J. Sato of Waseda University. The authors are indebted to I. Shimada for discussions on Lyapunov exponents.

Figure Captions

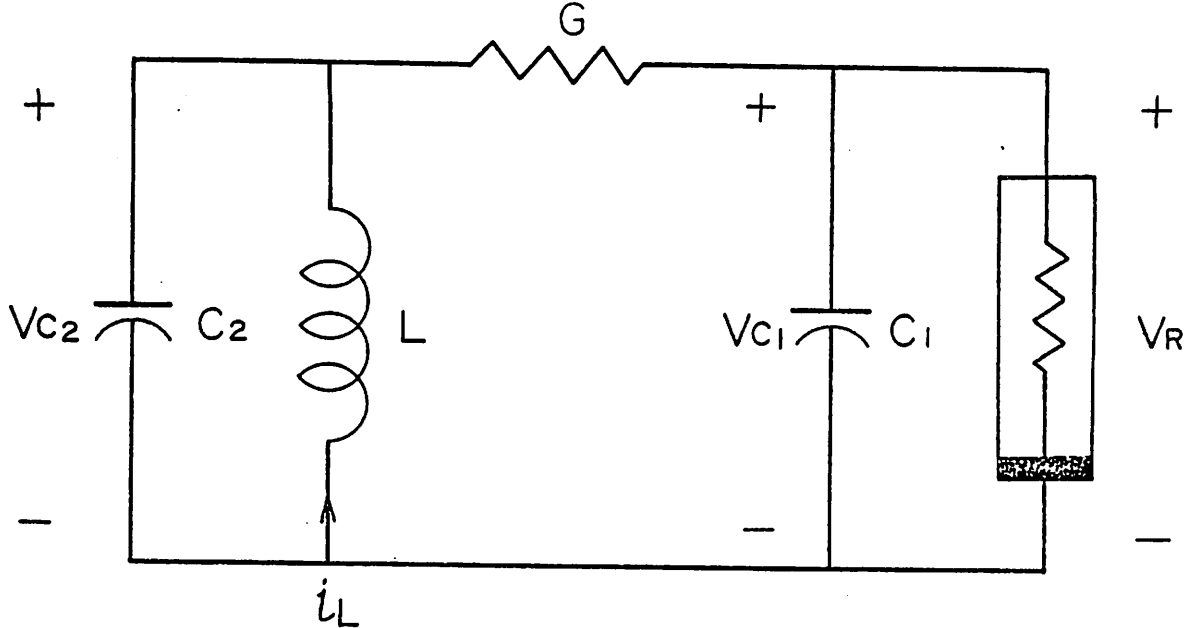
- Fig. 1. A simple autonomous circuit with a Chaotic attractor.
(a) The circuitry. (b) Constitutive relation of the resistor.
- Fig. 2. The Chaotic attractor and hyperbolic periodic orbit.
(a) Projection onto the (i_L, v_{C_1}) -plane. (b) Projection onto the (i_L, v_{C_2}) -plane. (c) Projection onto the (v_{C_1}, v_{C_2}) -plane. Runge-Kutta was iterated 10000 times with step size 0.04. Initial conditions: $v_{C_1}(0) = 0.15264$, $v_{C_2}(0) = -0.02281$, $i_L(0) = 0.38127$ for the attractor and $v_{C_1}(0) = 2.532735$, $v_{C_2}(0) = 1.285458 \times 10^{-3}$, $i_L(0) = -3.367482$ for the hyperbolic periodic orbit with period 3.54793. The length of each arrow is 2.5.
- Fig. 3. A modified constitutive relation of the resistor.
- Fig. 4. The large stable limit cycle with the chaotic attractor and hyperbolic periodic orbit. (a) Projection onto the (i_L, v_{C_1}) -plane. (b) Projection onto the (i_L, v_{C_2}) -plane. (c) Projection onto the (v_{C_1}, v_{C_2}) -plane. Initial conditions for the large stable limit cycle : $v_{C_1}(0) = -3.08832$, $v_{C_2}(0) = -1.0423$, $i_L(0) = 6.93155$ with period 2.87.
- Fig. 5. The chaotic attractor observed by a circuit realization: Projection onto the (v_{C_1}, v_{C_2}) -plane. Horizontal scale: 1V / division. Vertical scale: 1V / division.
- Fig. 6. Circuit realization. (a) The circuitry which realizes (1.1) with appropriate rescaling. The box with broken lines realizes g of Fig. 1(b). (b) Observed constitutive relation of g . Horizontal scale : 2V / division. Vertical scale : 2mA / division.

- Fig. 7. The chaotic attractor and hyperbolic periodic orbit observed with the set of parameter values (1.4). Initial conditions : $v_{C_1}(0)=1.45305$, $v_{C_2}(0) = -4.36956$, $i_L(0) = 0.15034$ for the attractor, and $v_{C_1}(0) = 10.00717$, $v_{C_2}(0) = 1.80100$, $i_L(0) = -23.90375$ for the hyperbolic periodic orbit with period 3.93165. The length of each arrow is 15.
- Fig. 8. The chaotic attractor and hyperbolic periodic orbit with the smooth resistor constitutive relation (1.5). Initial conditions : $v_{C_1}(0) = 1.47147$, $v_{C_2}(0) = 0.83242$, $i_L(0) = 2.23418$ for the attractor, and $v_{C_1}(0) = 9.998048$, $v_{C_2}(0) = 1.980972$, $i_L(0) = -10.908448$ for the hyperbolic periodic orbit with period 4.49. The length of each arrow is 11.
- Fig. 9. Eigen spaces of the equilibria and related sets.
- Fig. 10. Description of typical trajectories in the attractor.
- Fig. 11. Deformations of a rectangle along a trajectory.
- Fig. 12. Geometric structure of the attractor.
- Fig. 13. Cross sections of the attractor. (a) Locations of cross sections. (b) Cross section at $v_{C_1} = 0.00$. (c) Cross section at $v_{C_1} = 0.25$. (d) Cross section at $v_{C_1} = 0.50$. (e) Cross section at $v_{C_1} = 0.75$. (f) Cross section at $v_{C_1} = 1.00$ with related sets. (g) Cross section at $v_{C_1} = 1.25$. (h) Cross section at $v_{C_1} = 1.50$. (i) Cross section at $v_{C_1} = 1.75$. (j) Cross section at $v_{C_1} = 2.00$. (k) Cross section at $v_{C_1} = 2.20$. All of them have the same scaling.
- Fig. 14. A detailed geometric model for the attractor.
- Fig. 15. Characteristic exponents for periodic orbits. (a) Stable limit cycle. (b) Hyperbolic periodic orbit.

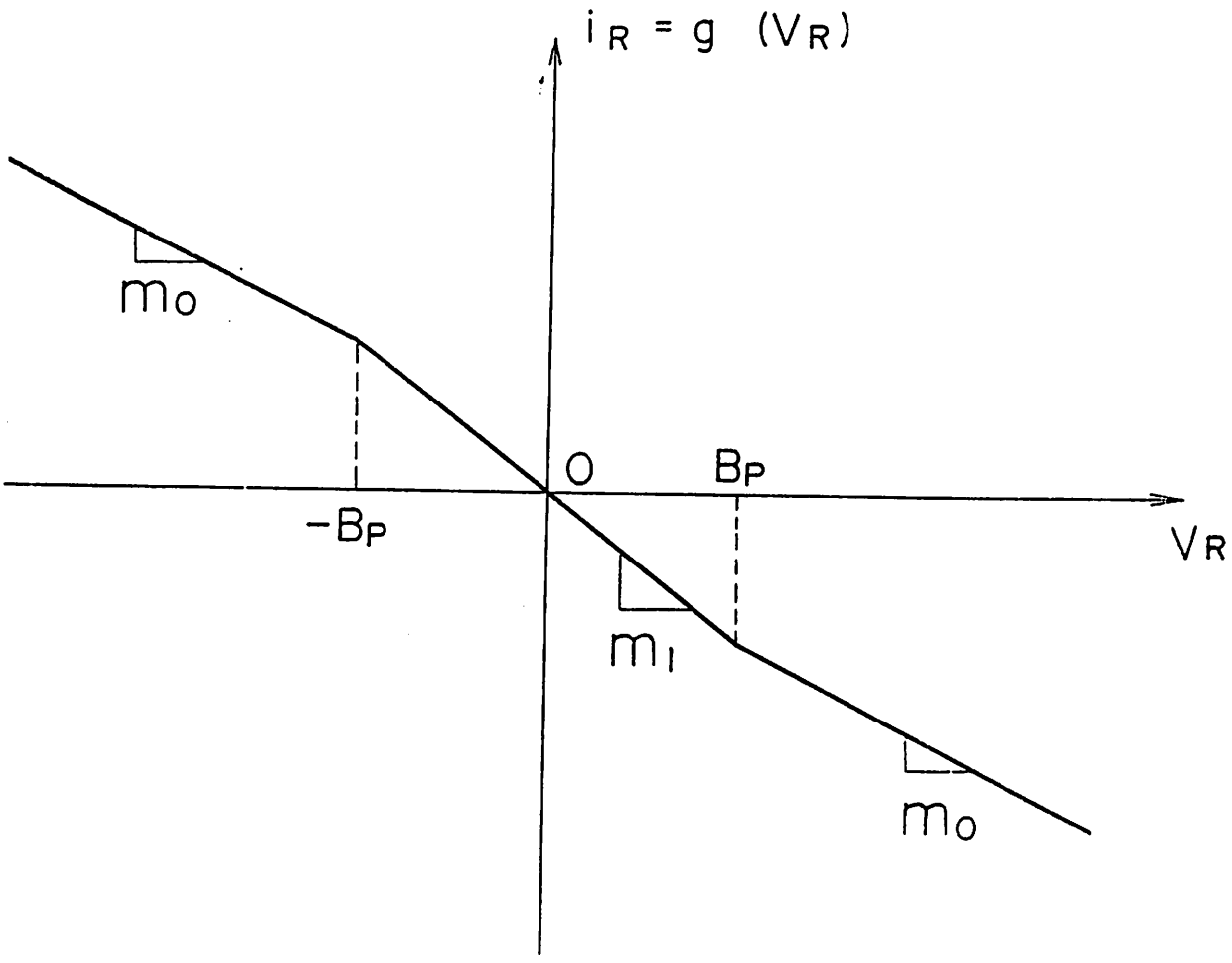
Fig. 16. Power spectra for the three state variables: (a) v_{C_1} , (b) v_{C_2} ,
(c) i_L . Vertical scale : 10 dB/division. Horizontal axis :
normalized frequency.

Fig. 17. Power spectra observed with the circuit of Fig. 6 : (a) v_{C_1} , (b) v_{C_2} .

Fig. 18. 1-dimensional map for i_L at the cross section $v_{C_1} = -1.6$.



(a)



(b)

Fig. 1

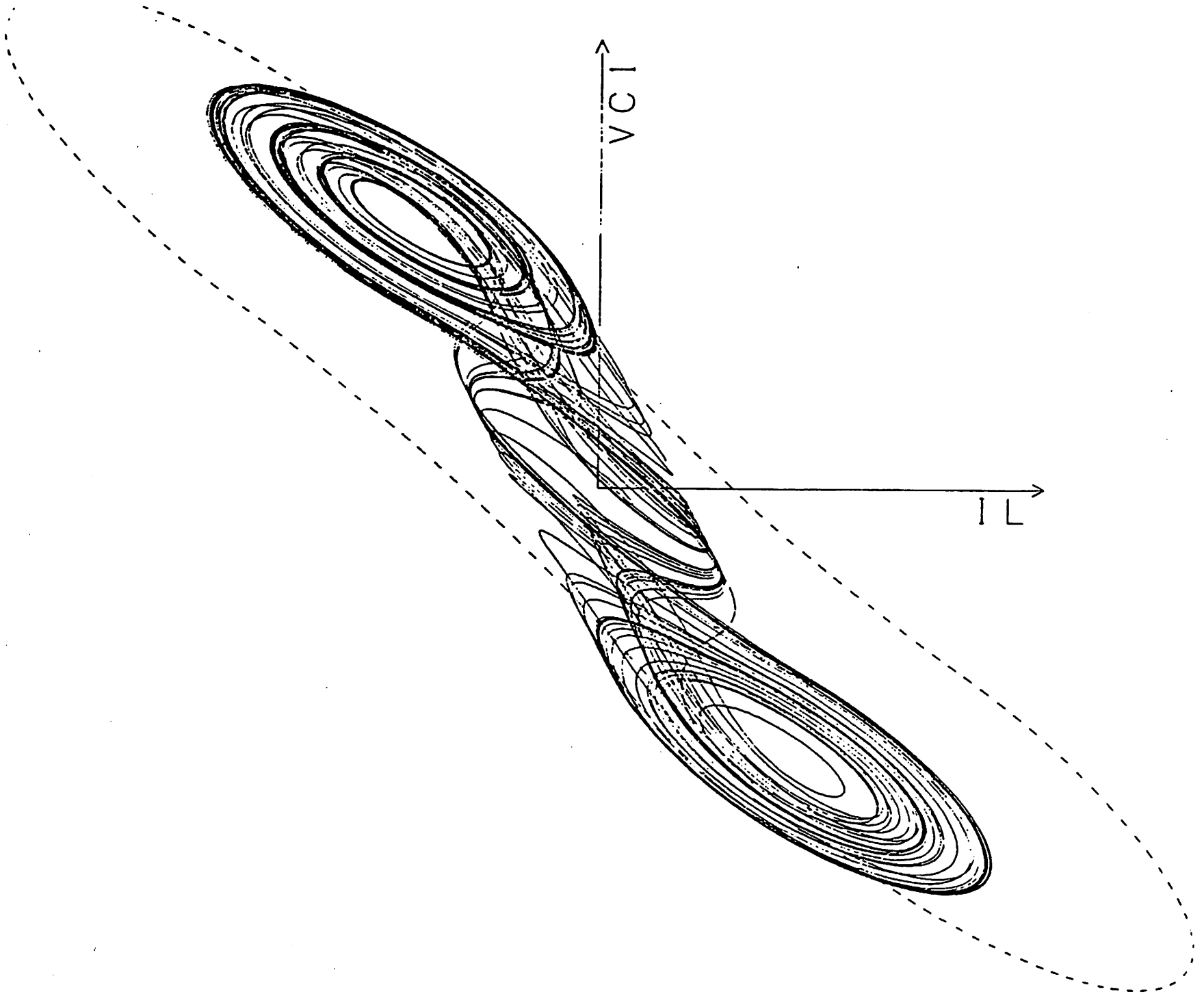


Fig. 2(a)

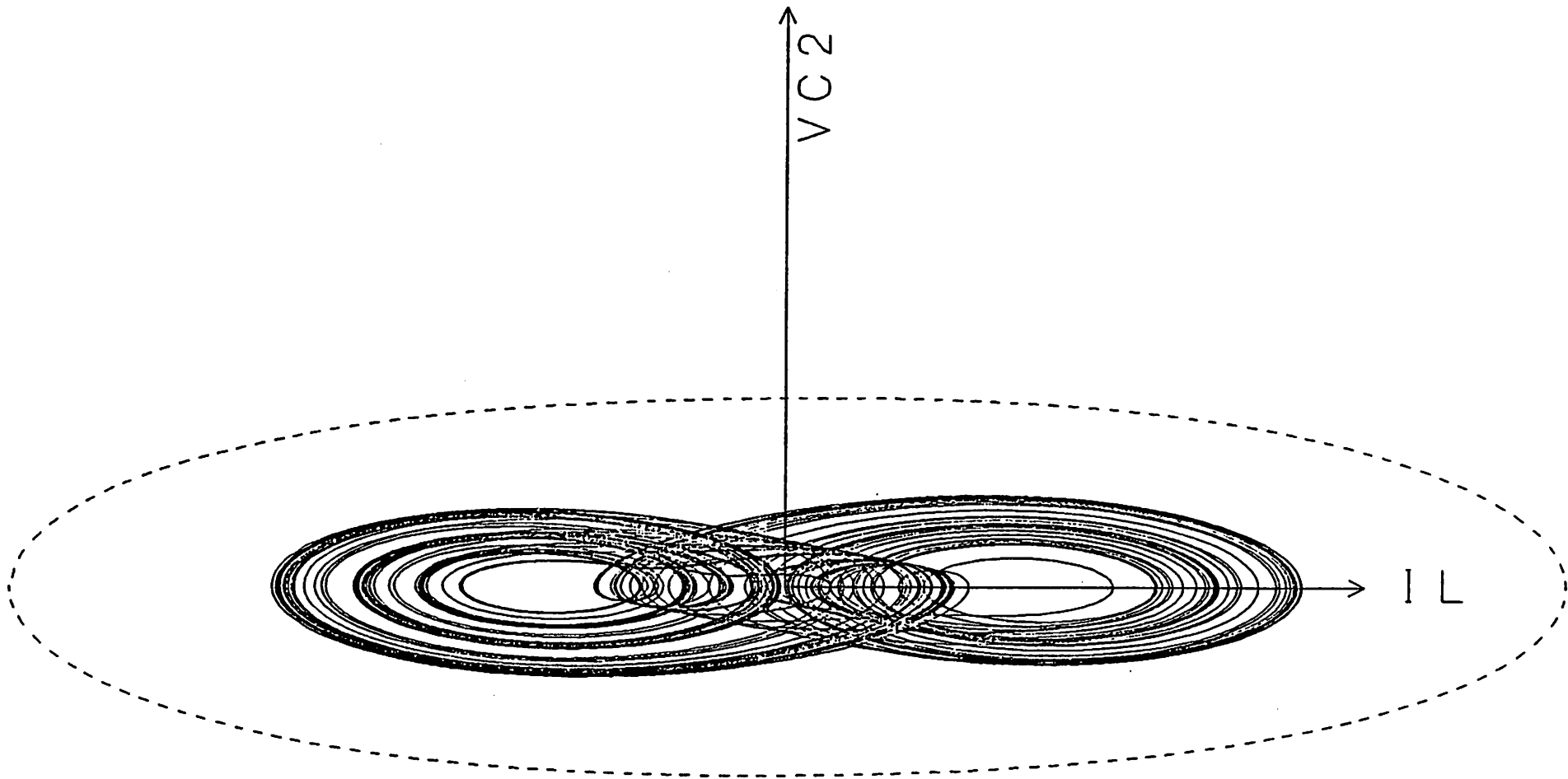


Fig. 2(b)

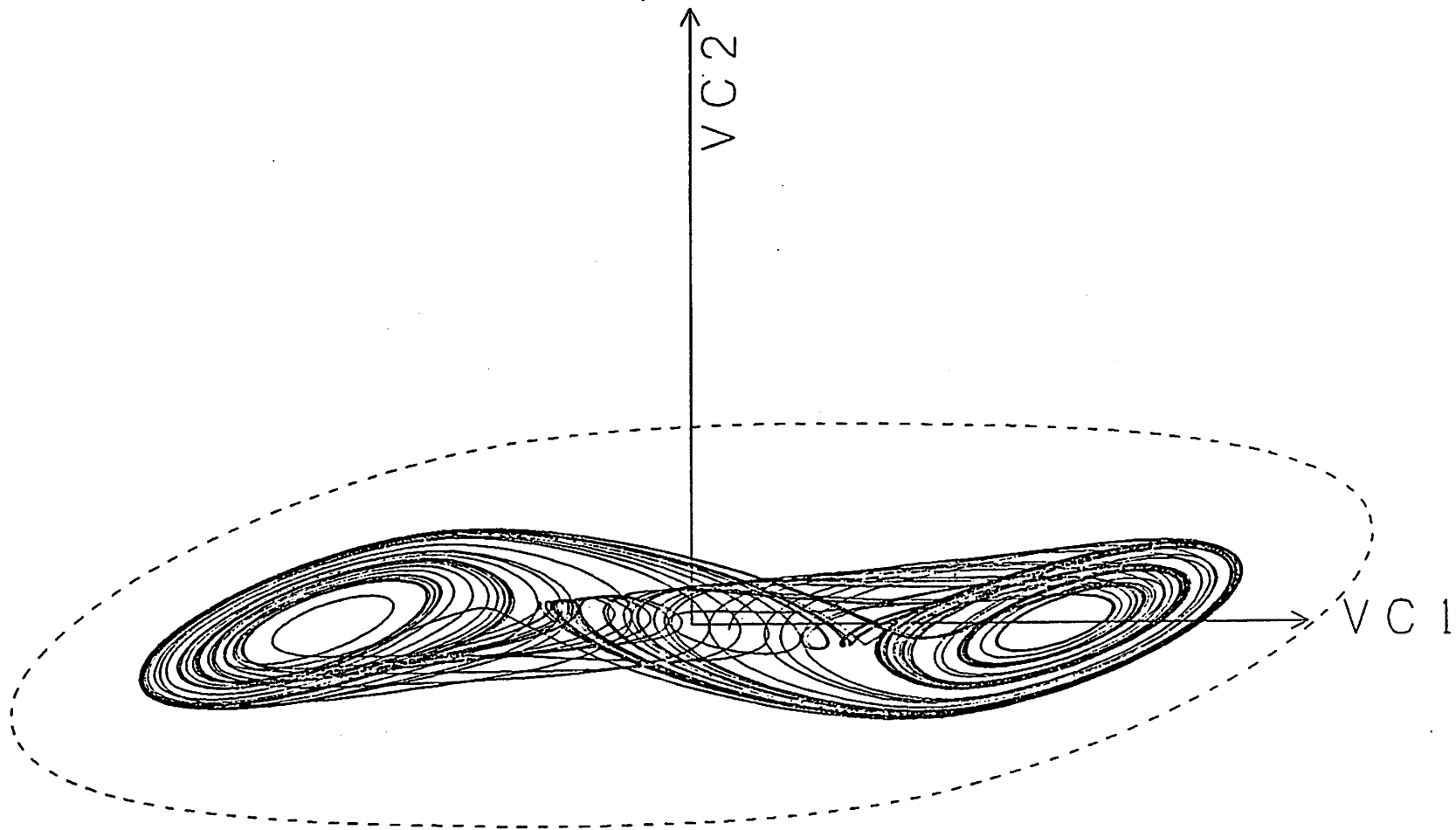


Fig. 2(c)

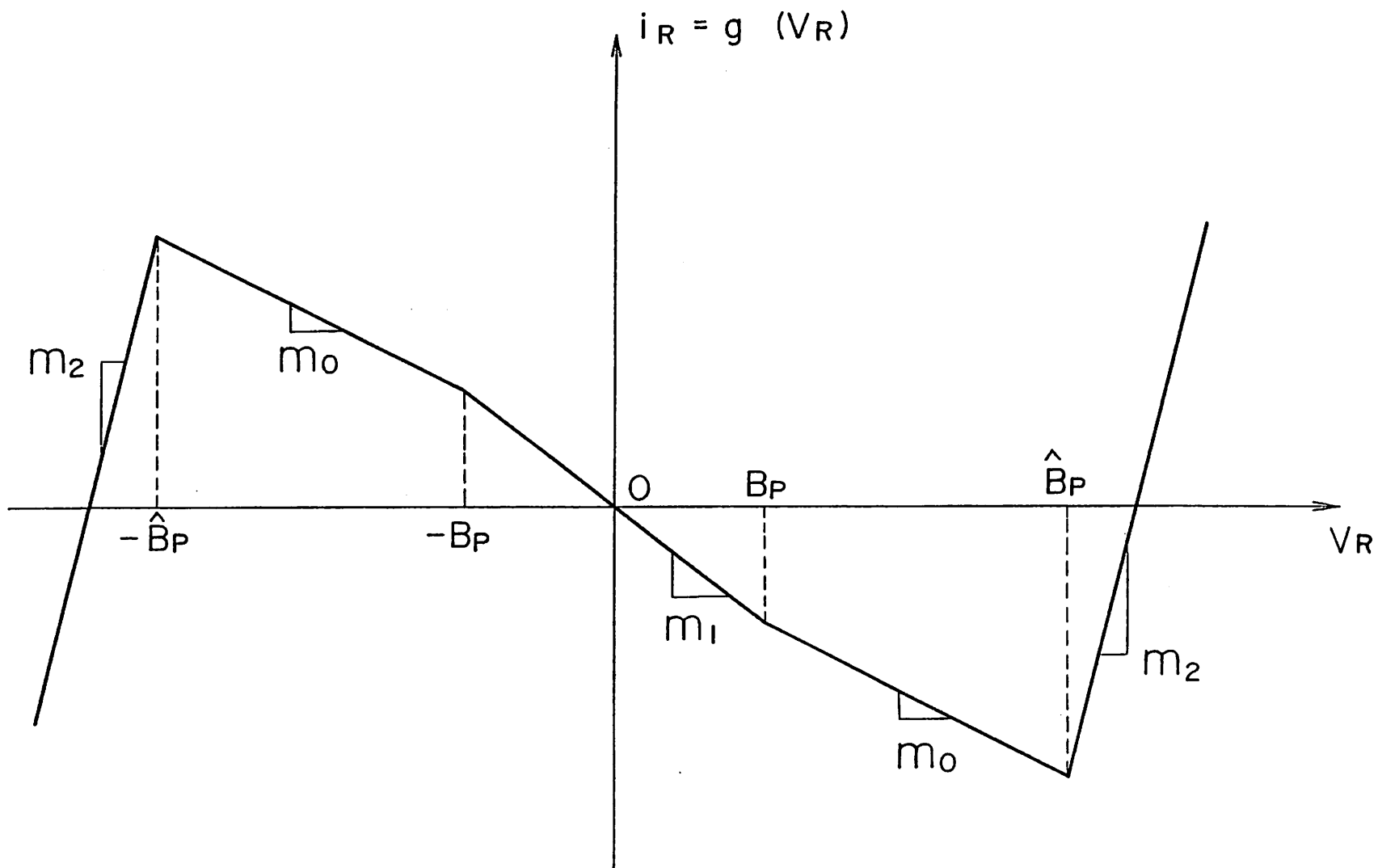


Fig. 3

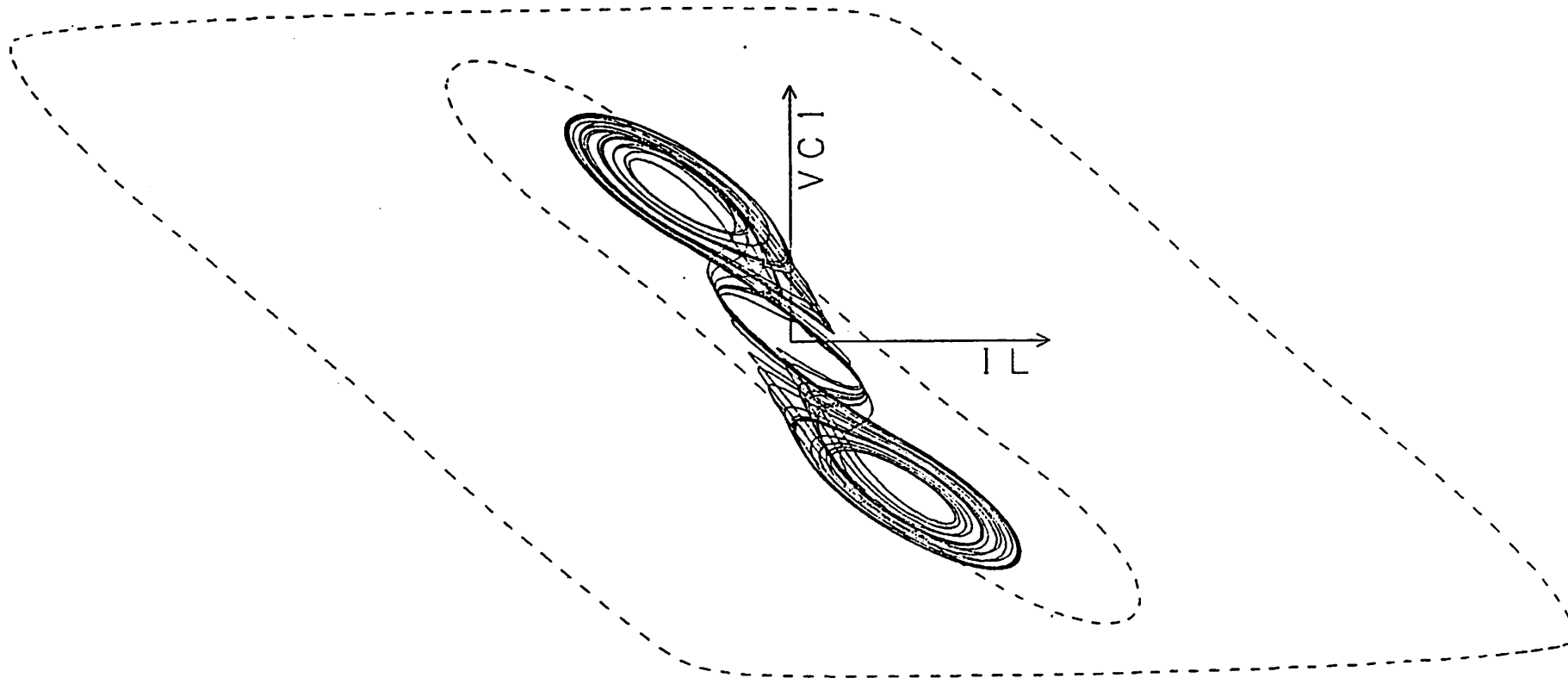


Fig. 4(a)

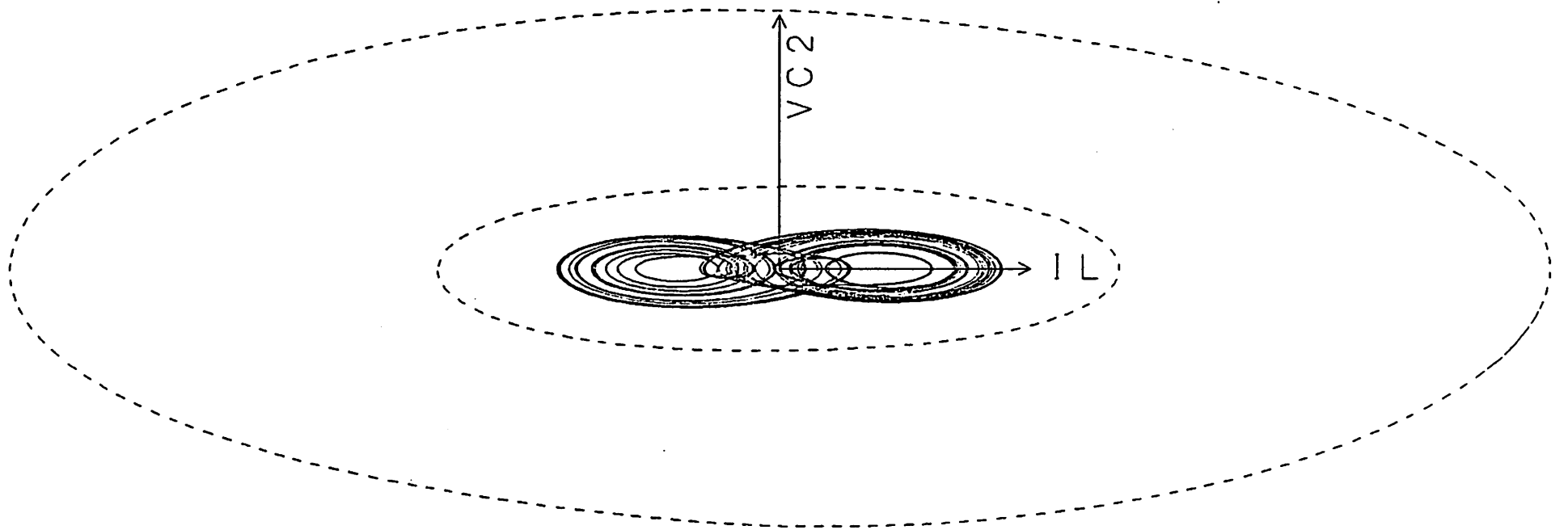


Fig. 4(b)

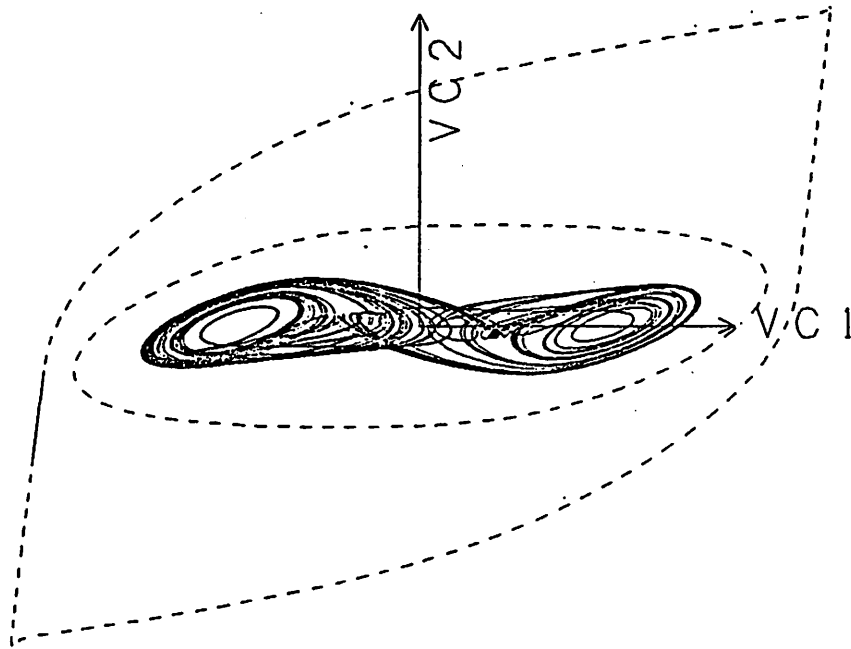


Fig. 4(c)

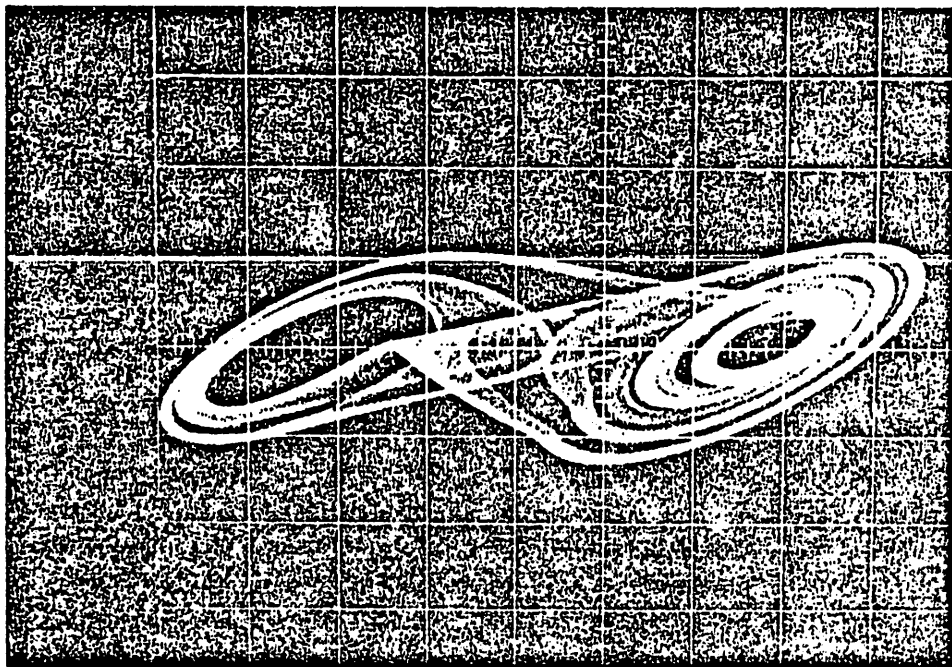


Fig. 5

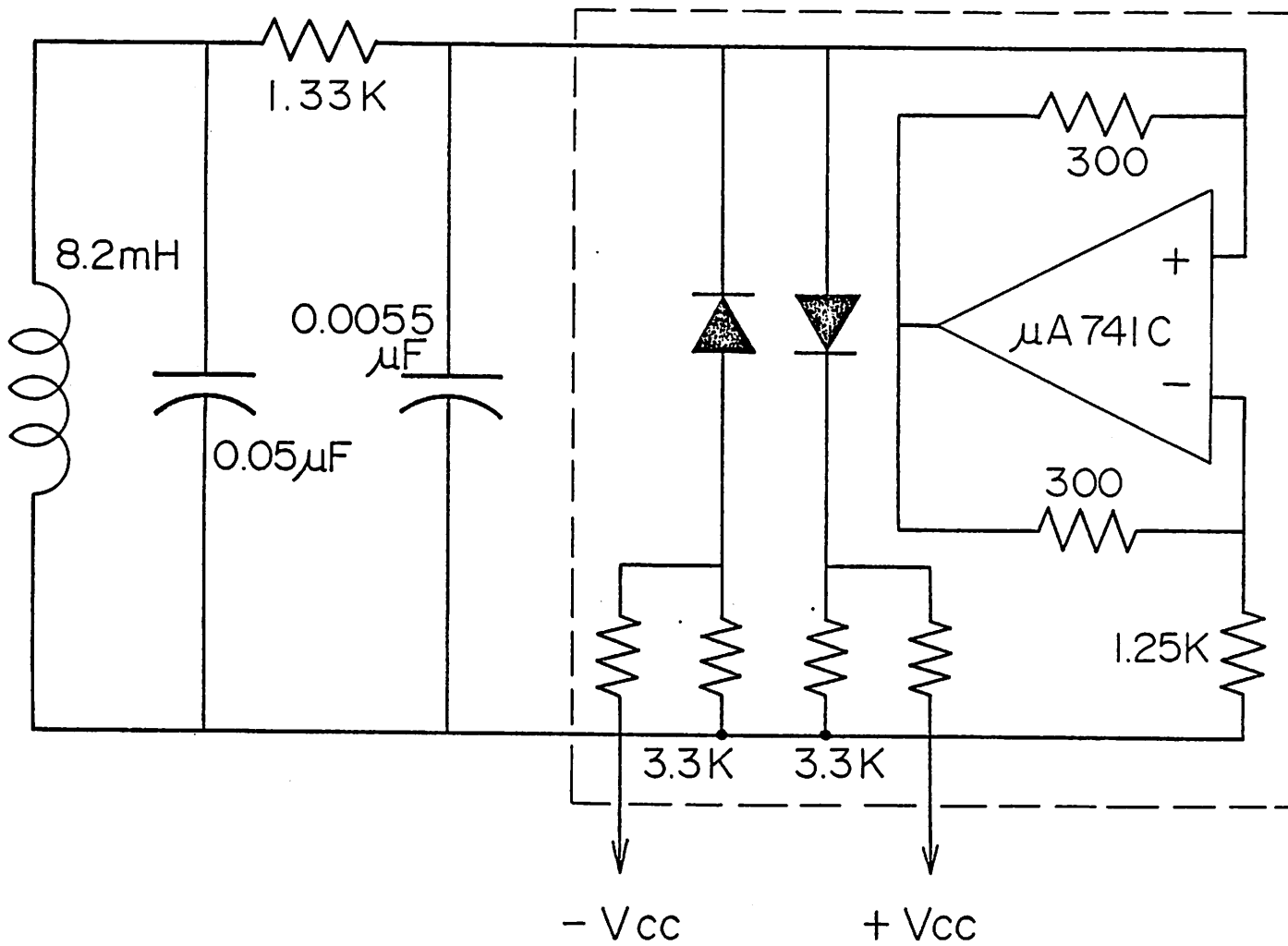
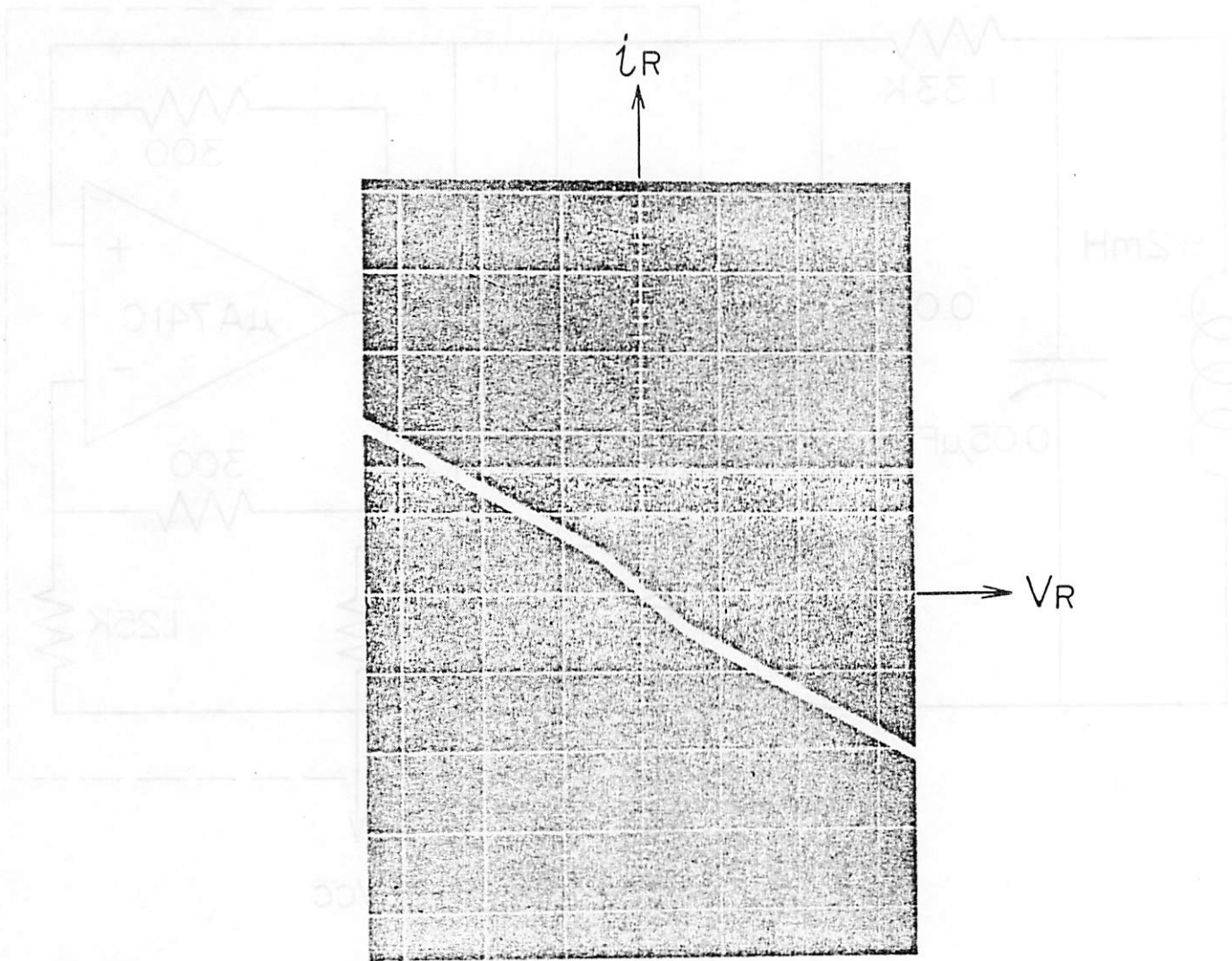


Fig 6 (a)



(a) 3 919

Fig. 6 (b)

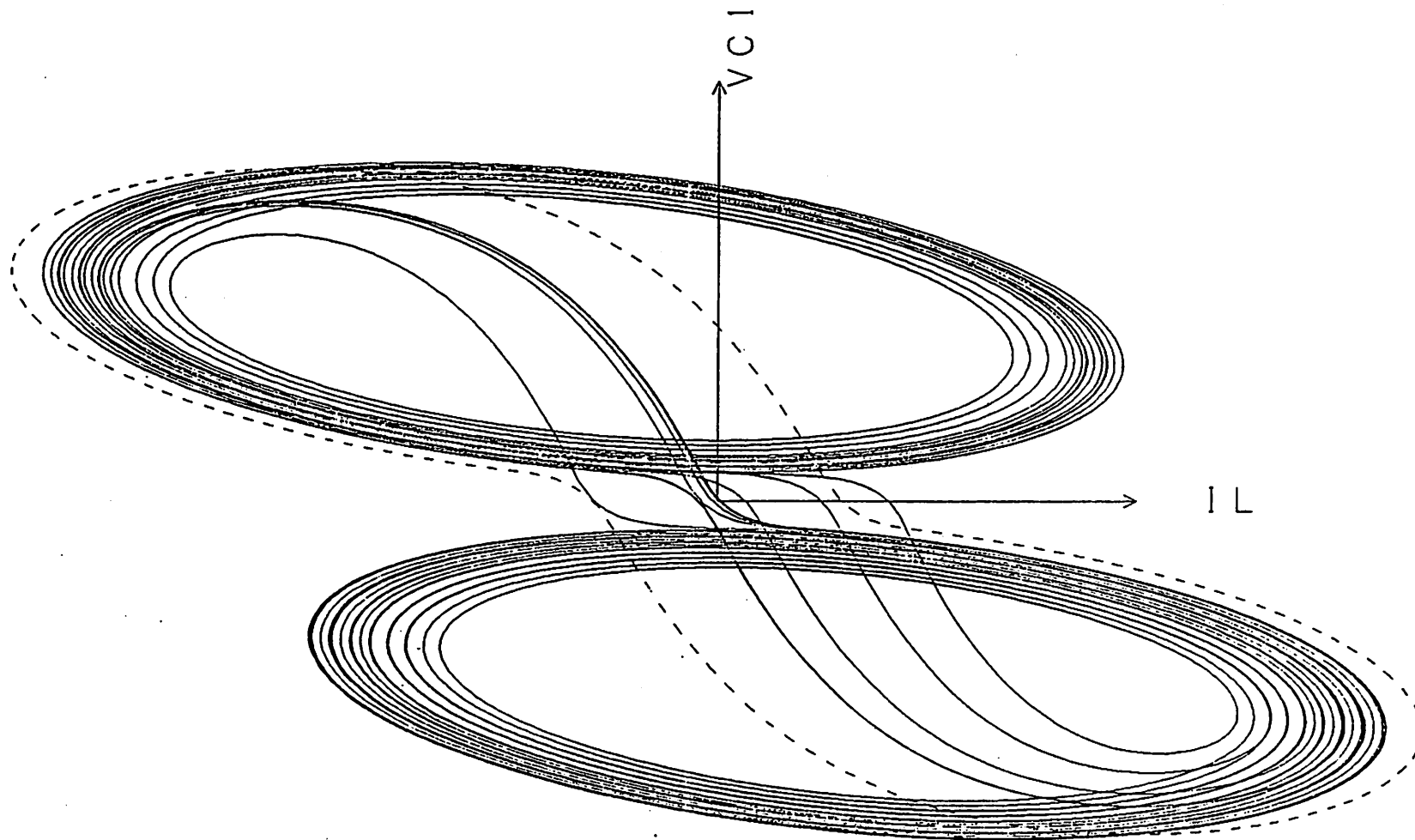


Fig. 7

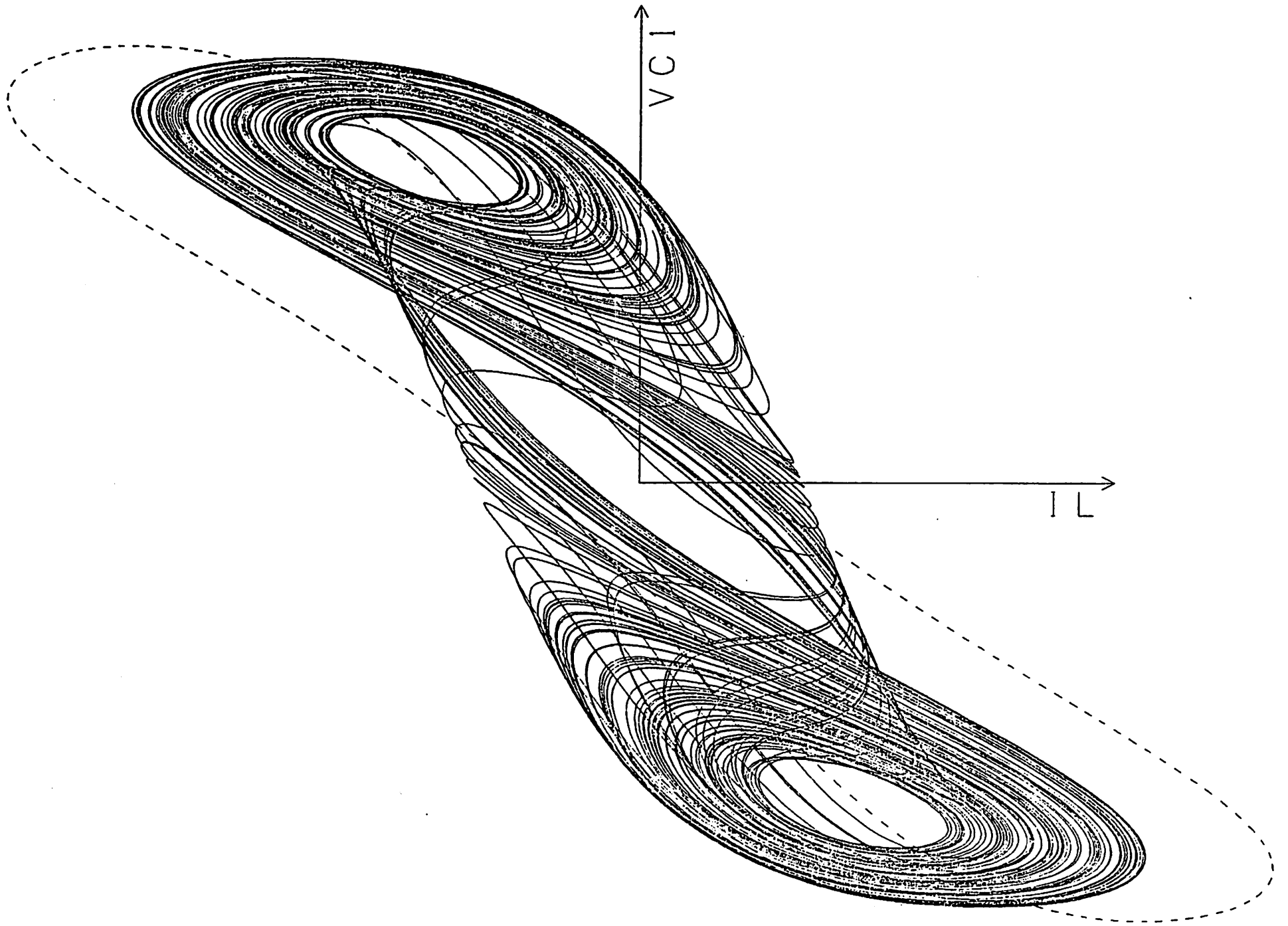


Fig. 8

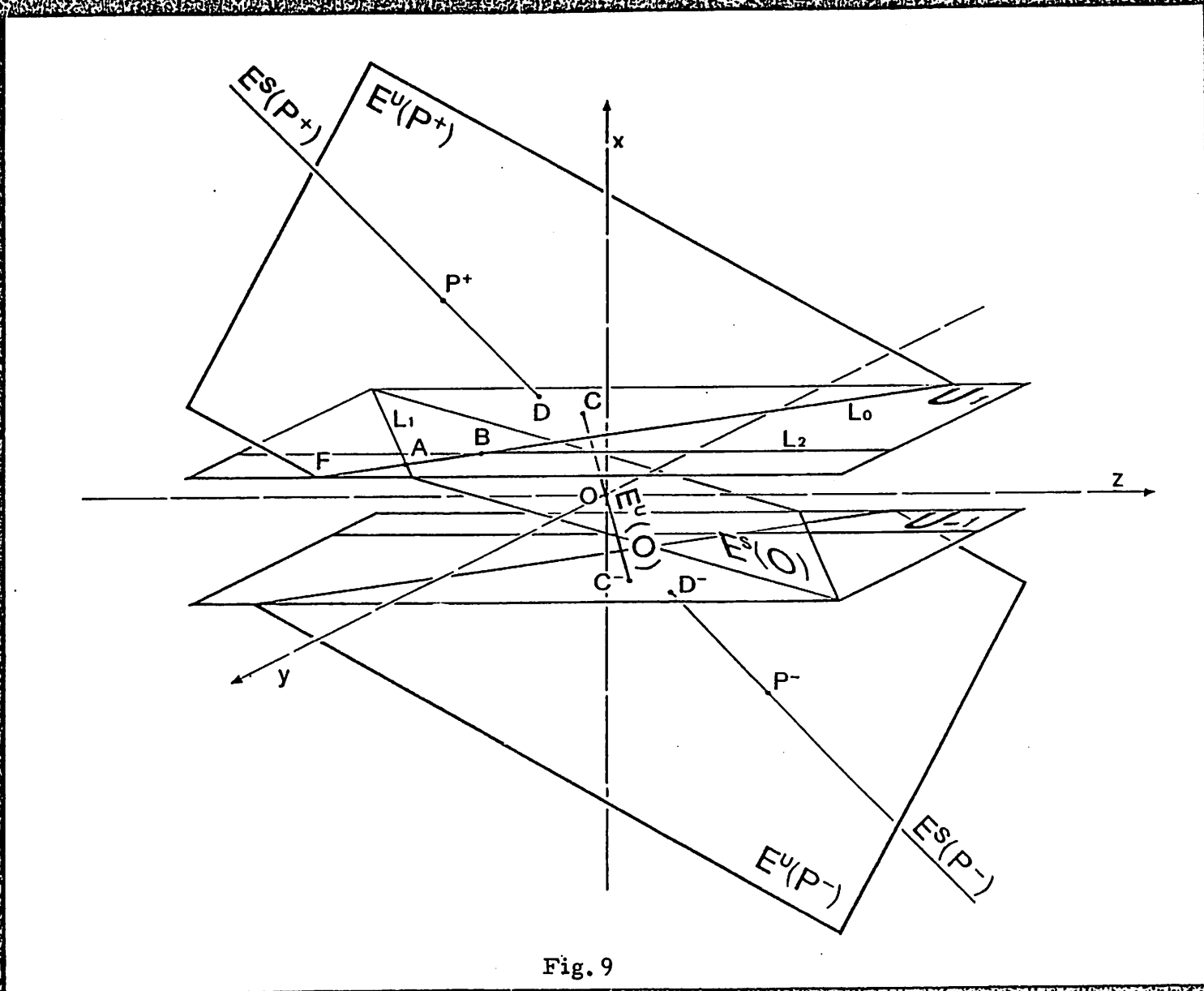


Fig. 9

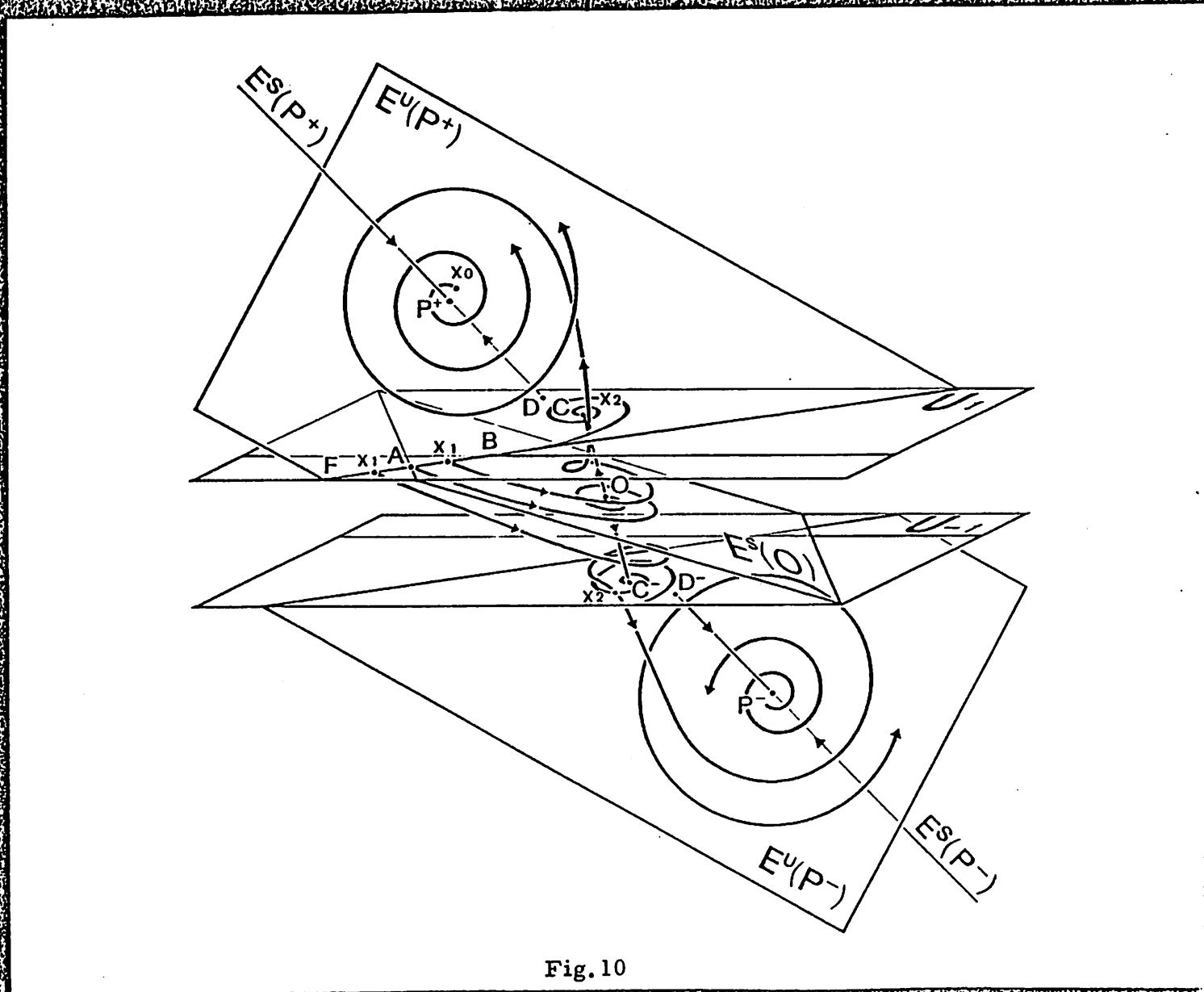


Fig. 10

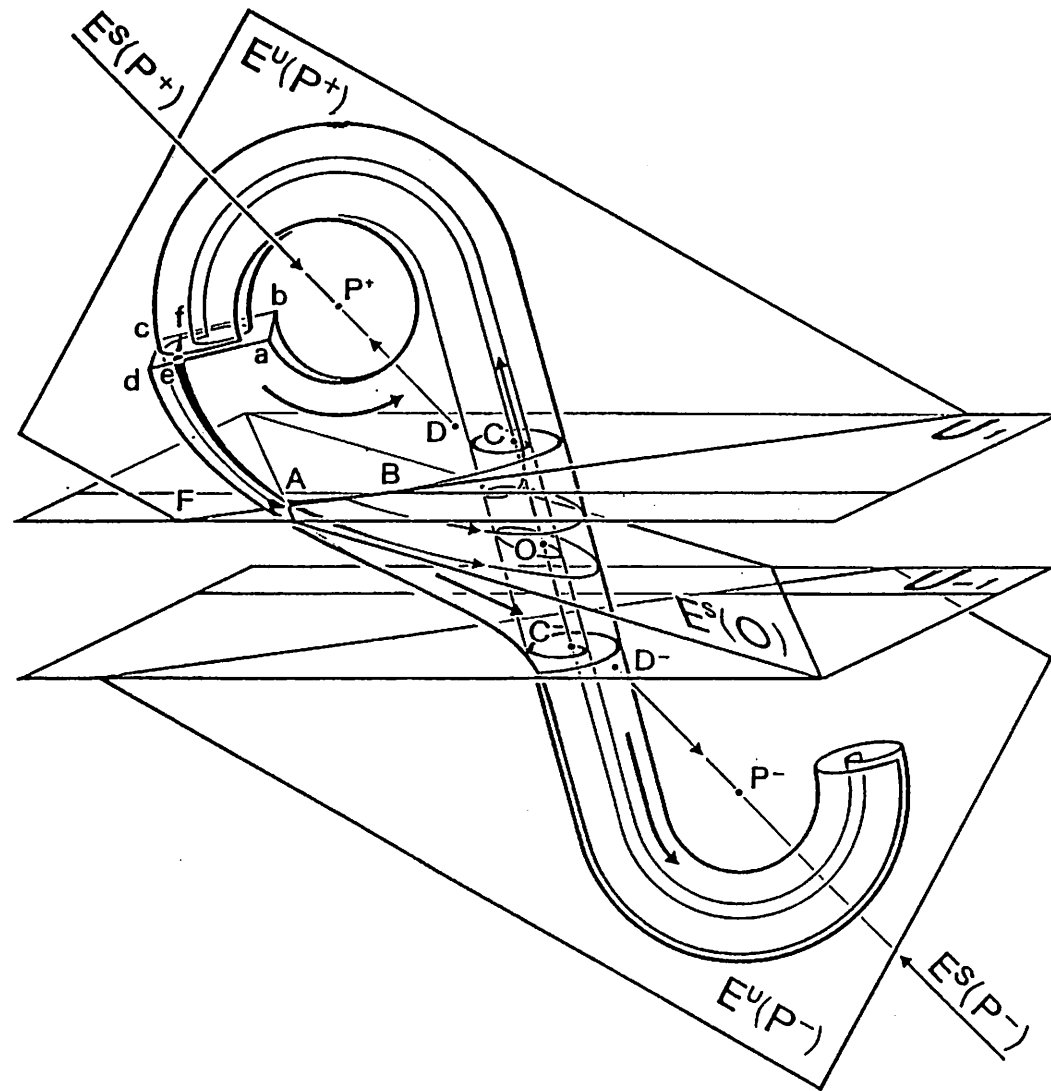


Fig. 11

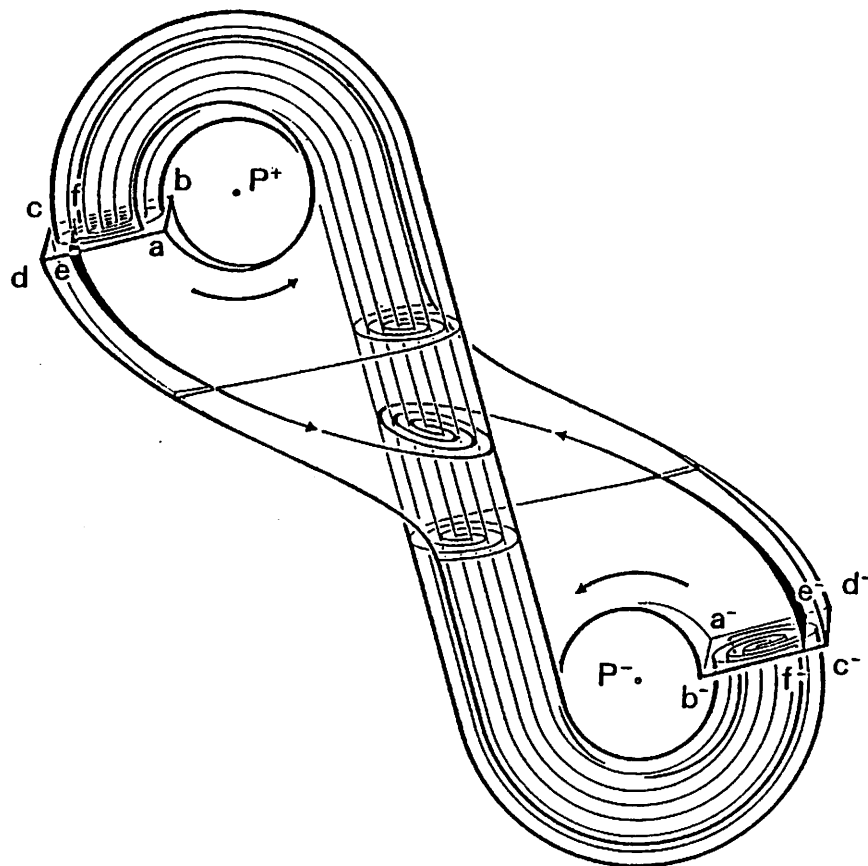


Fig. 12

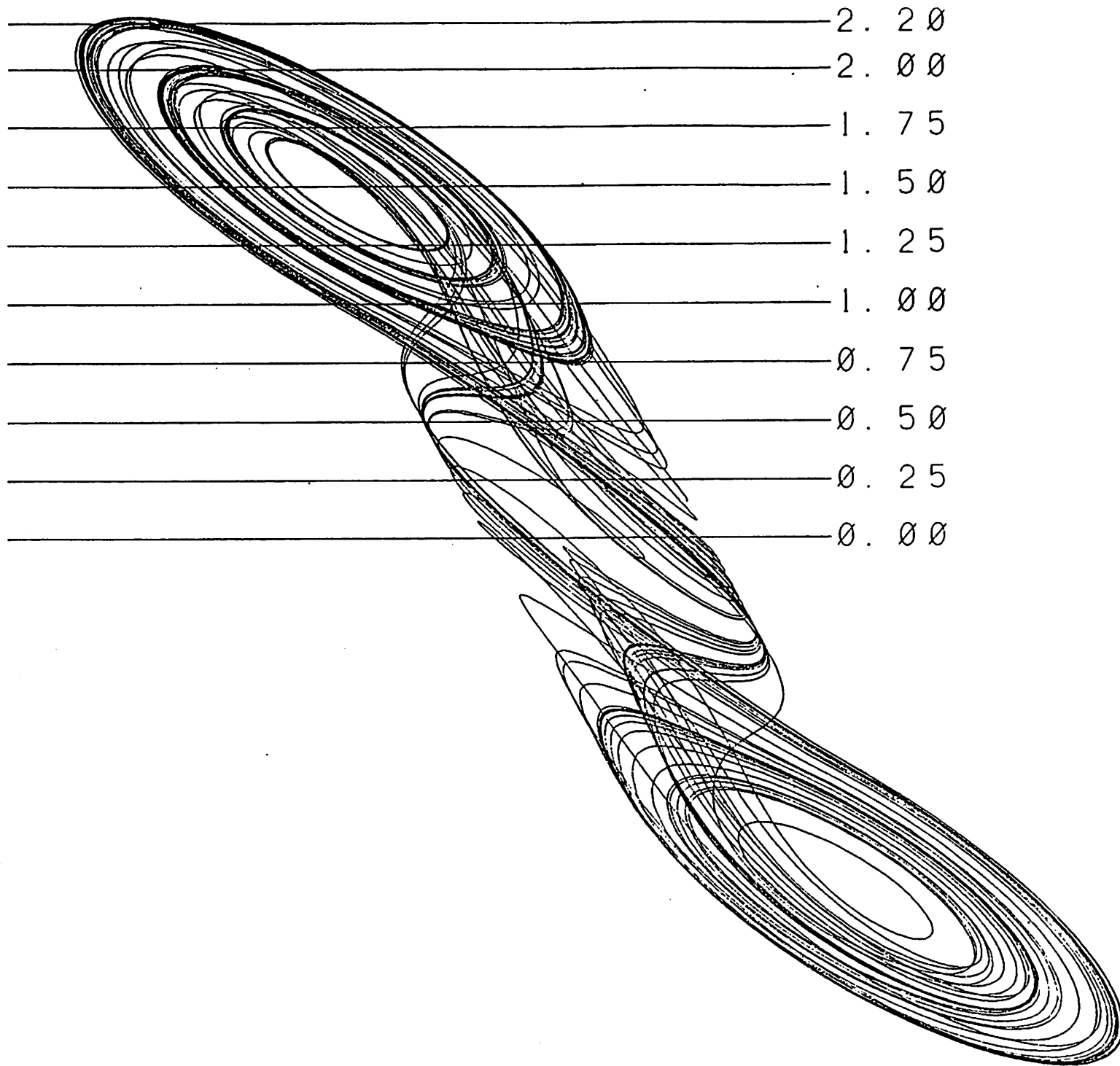


Fig. 13(a)

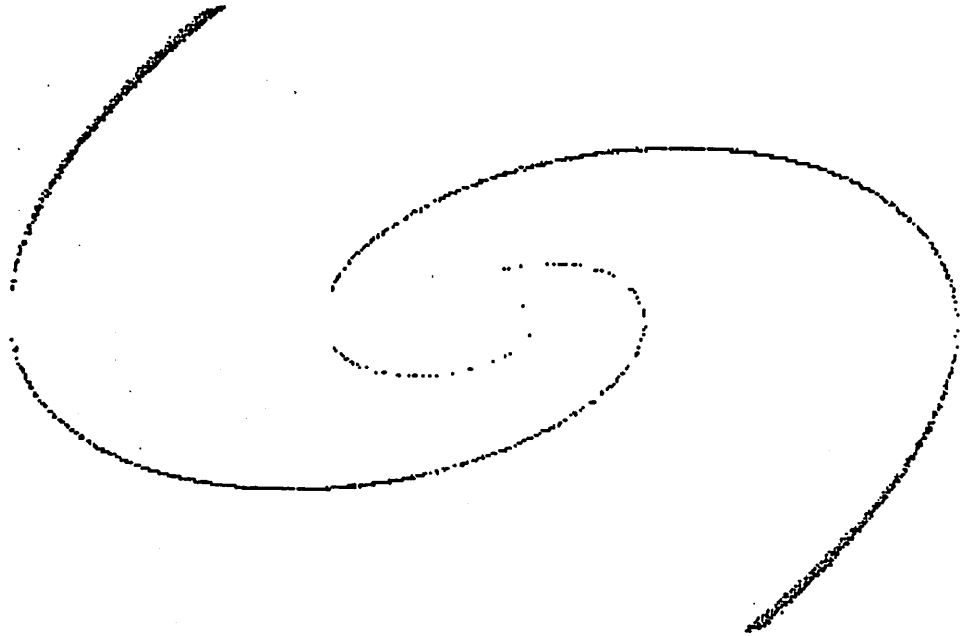


Fig. 13(b)

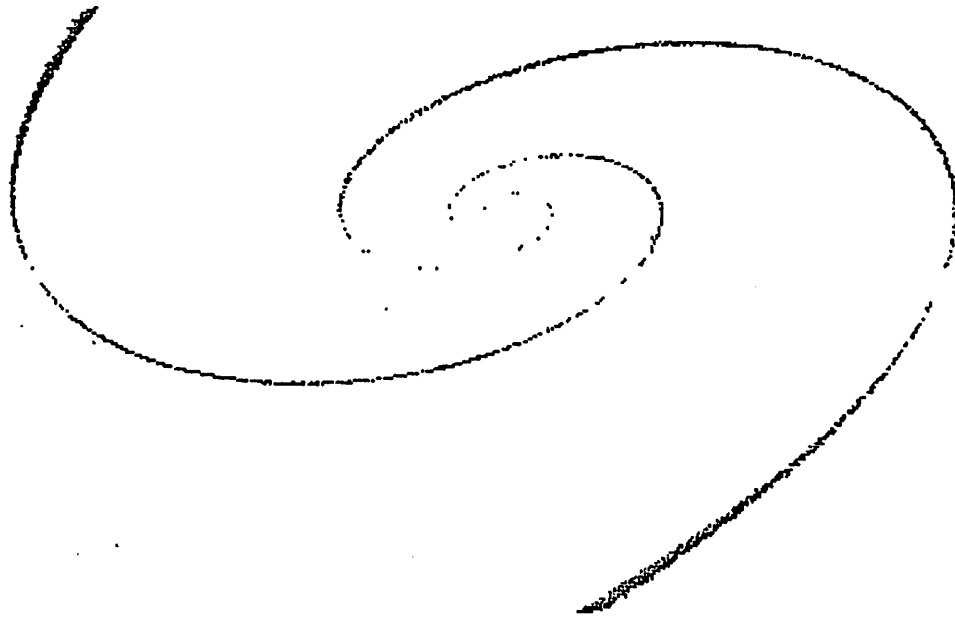


Fig.13(c)

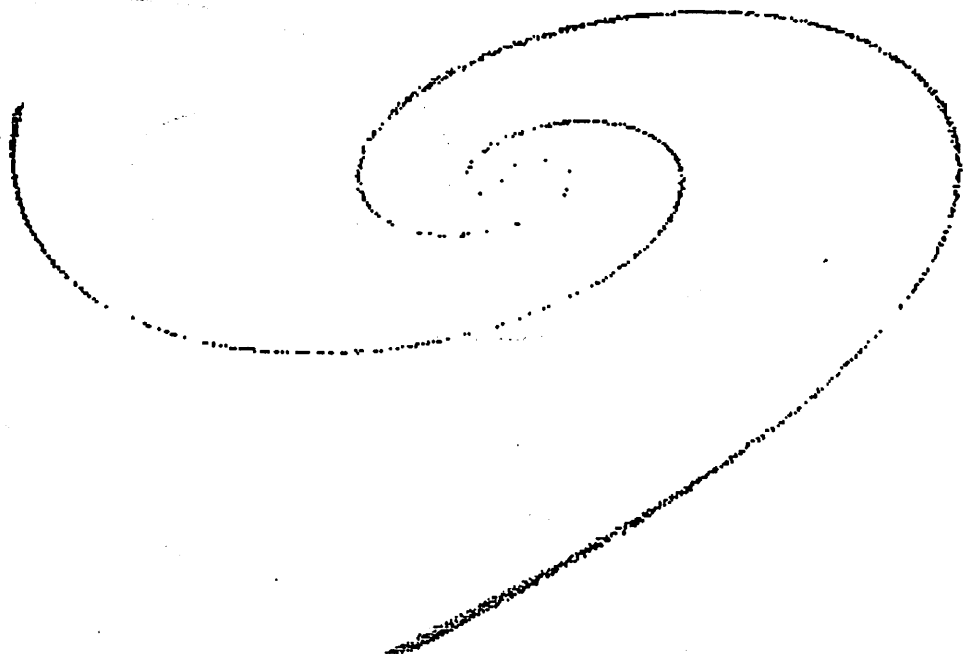


Fig. 13(d)

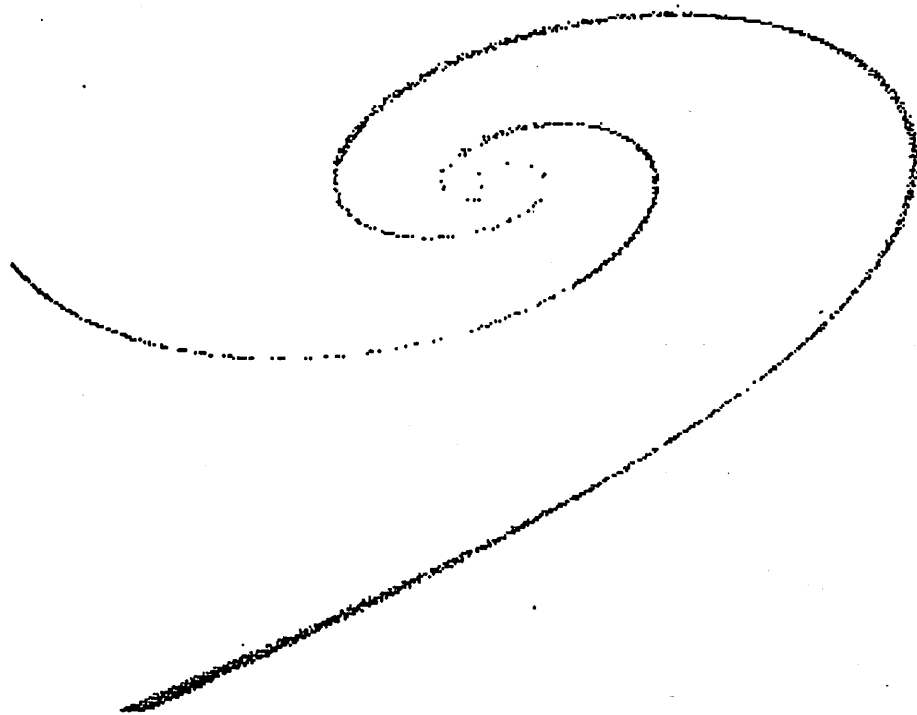


Fig. 13(e)

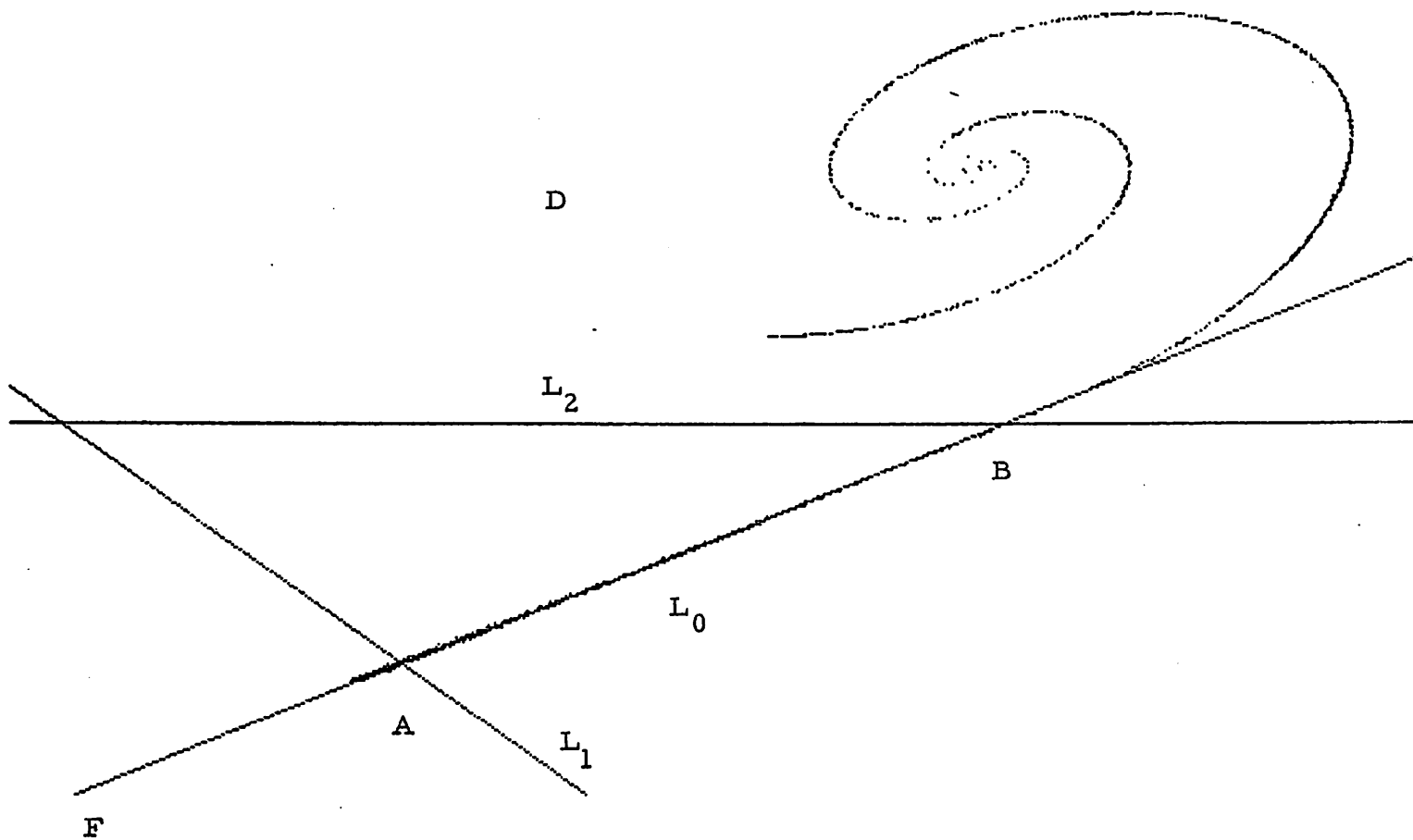


Fig. 13(f)

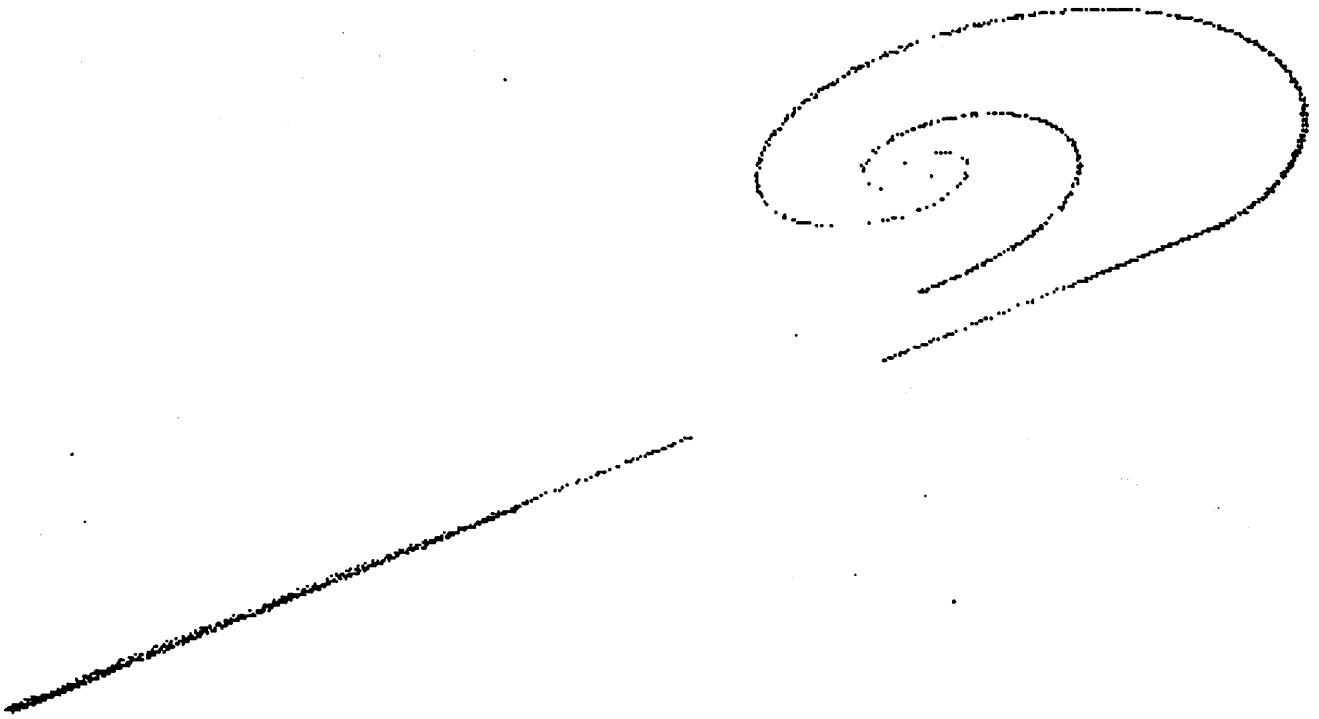


Fig. 13(g)

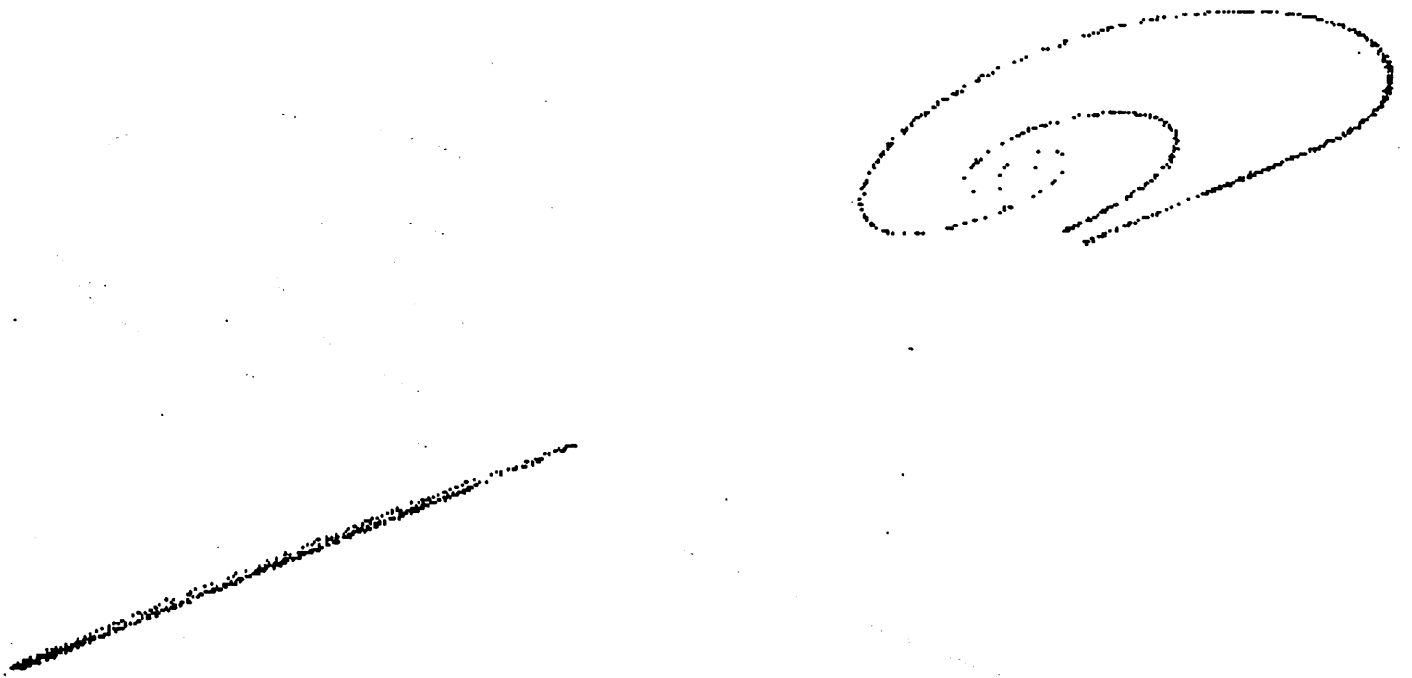


Fig. 13(h)

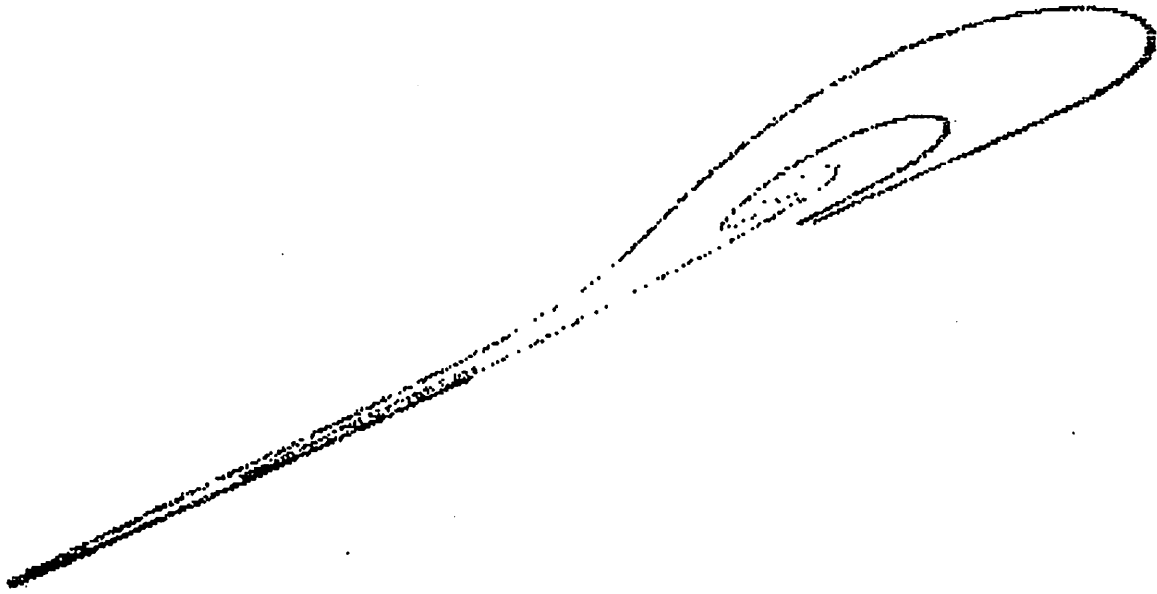


Fig. 13(i)

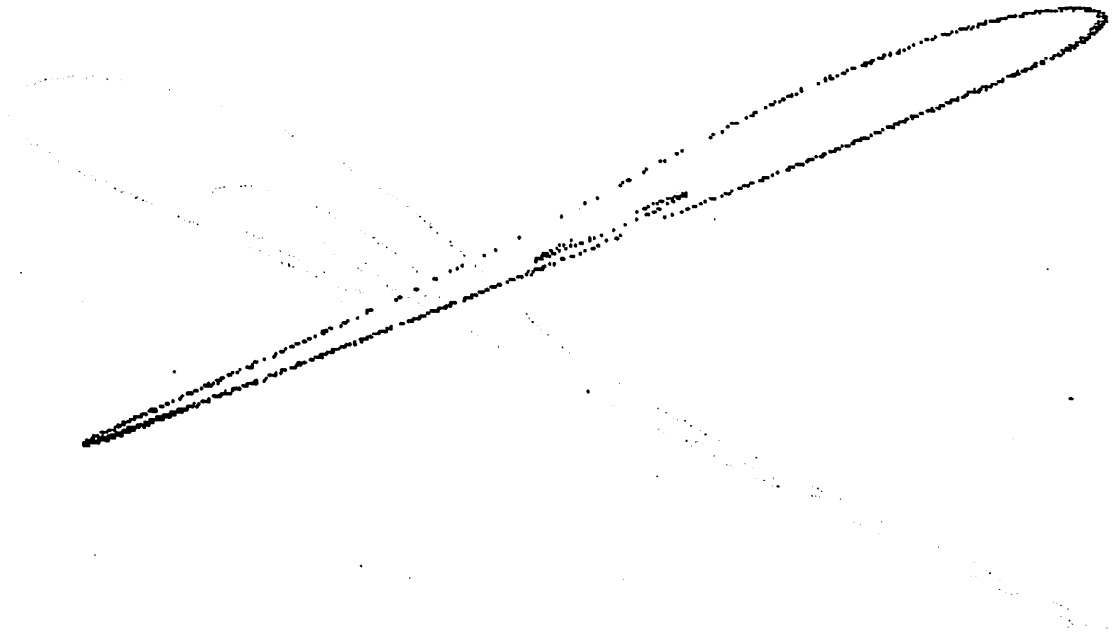


Fig. 13(j).

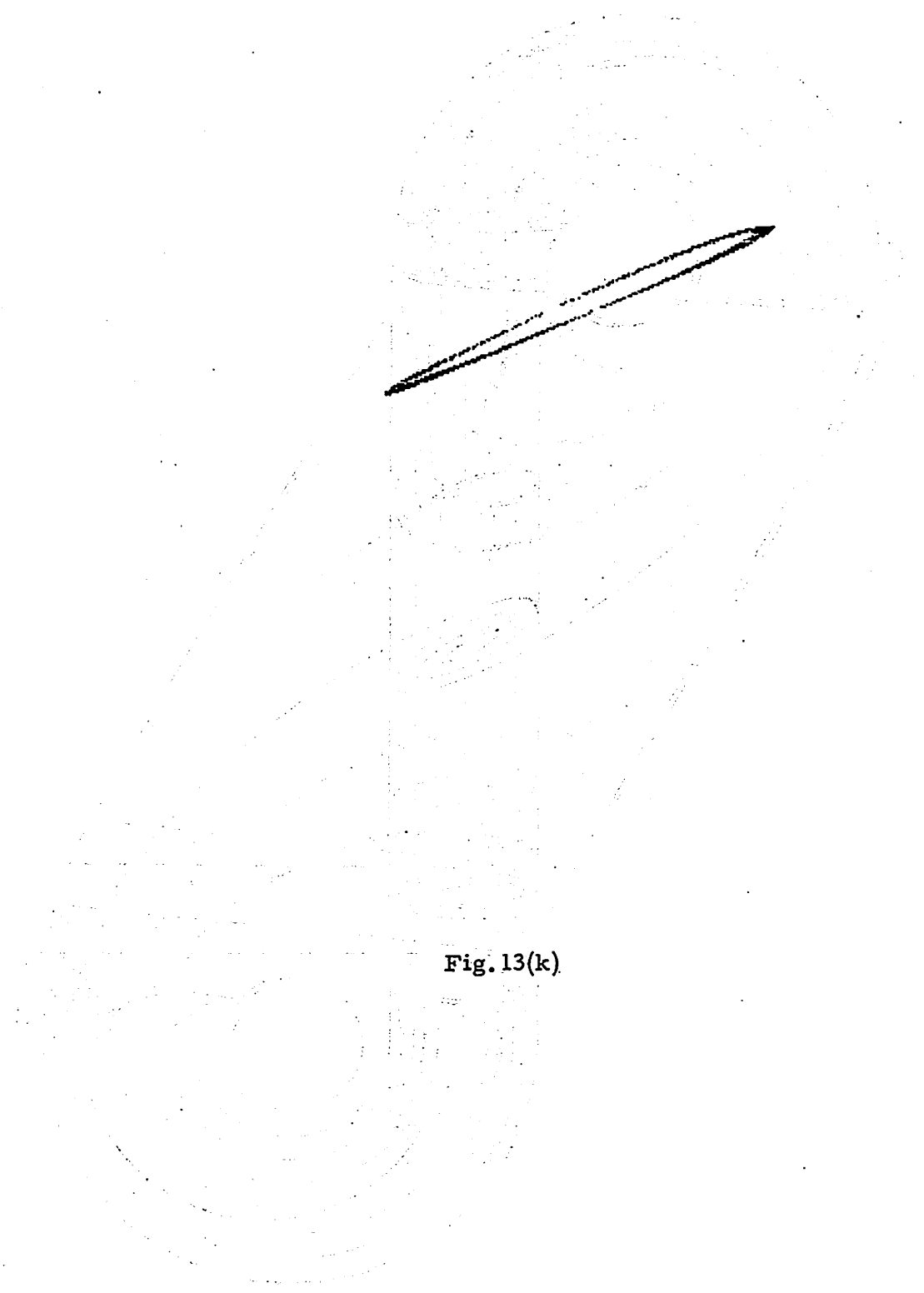


Fig. 13(k)

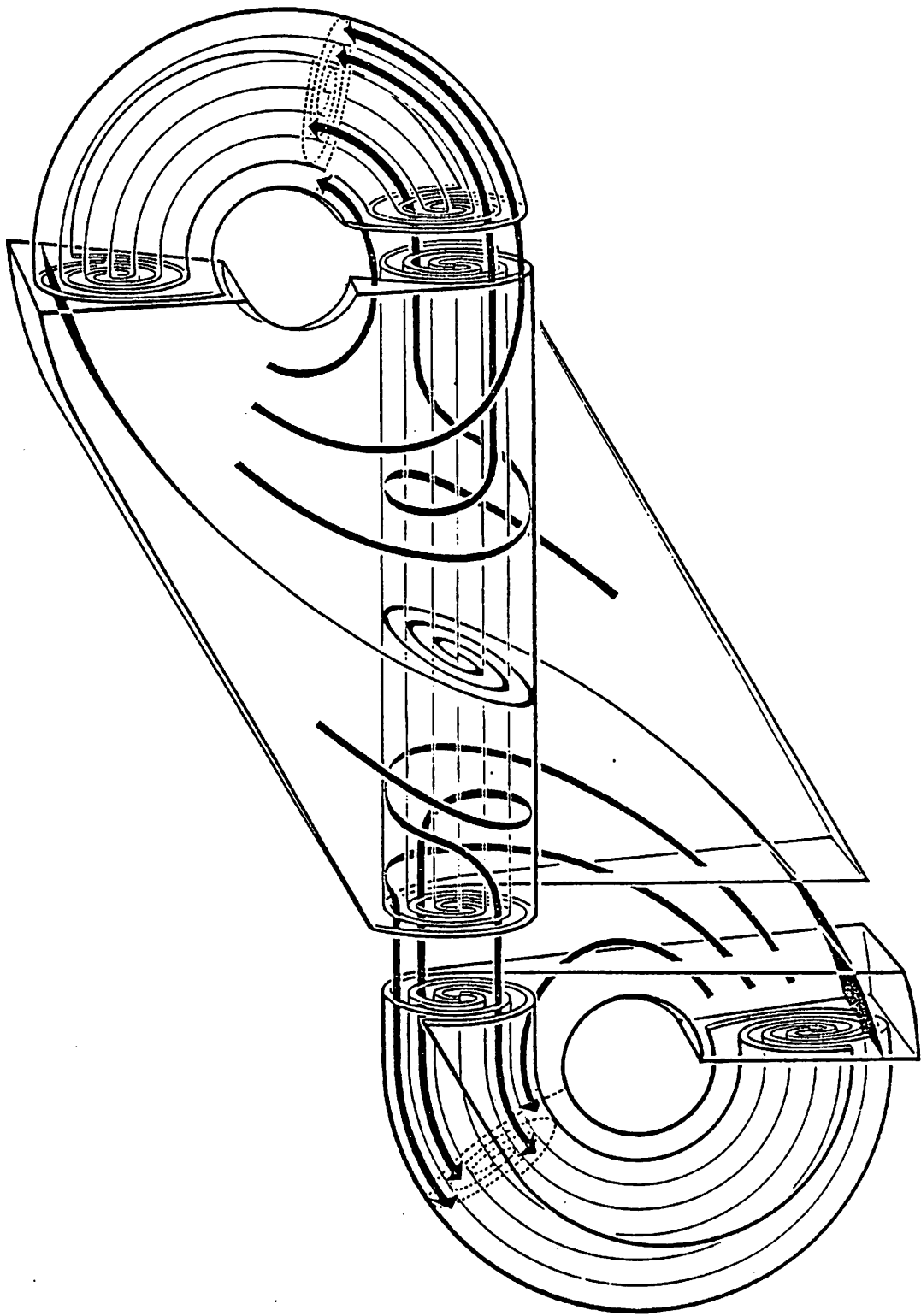
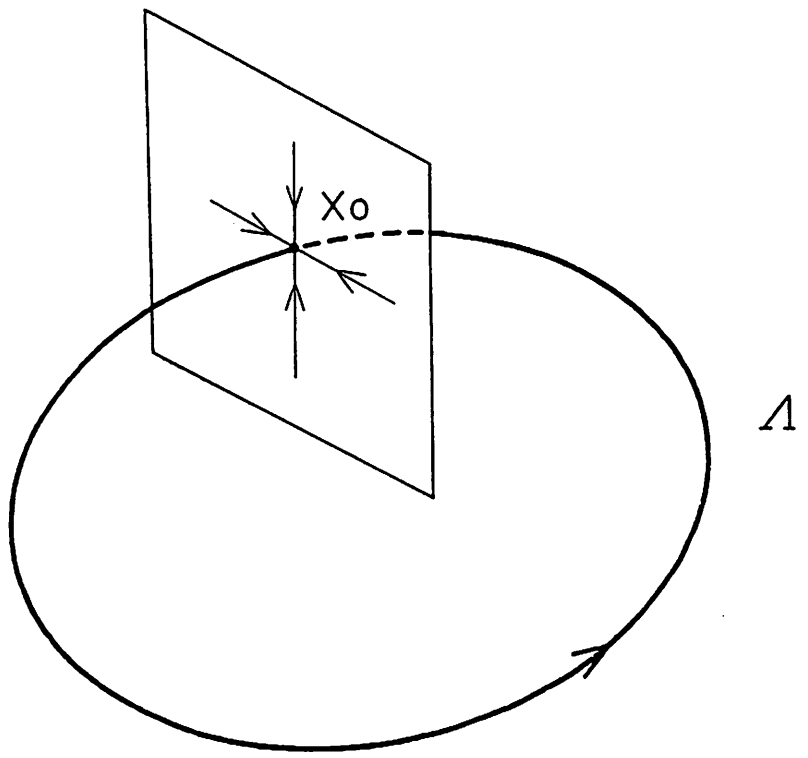
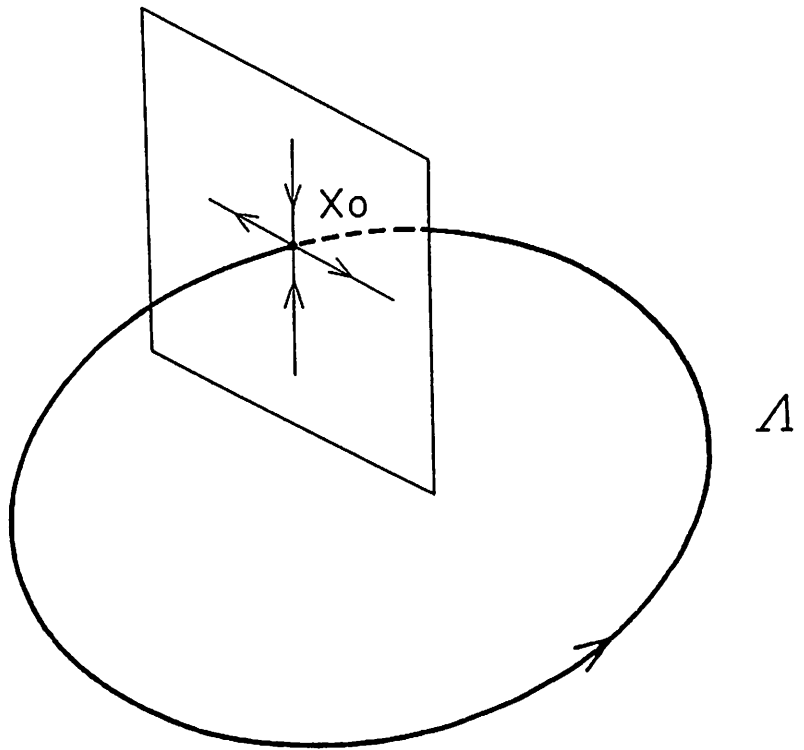


Fig. 14



(a)



(b)

Fig. 15

POWER SPECTRUM FOR VC1
LOG-LOG SCALE

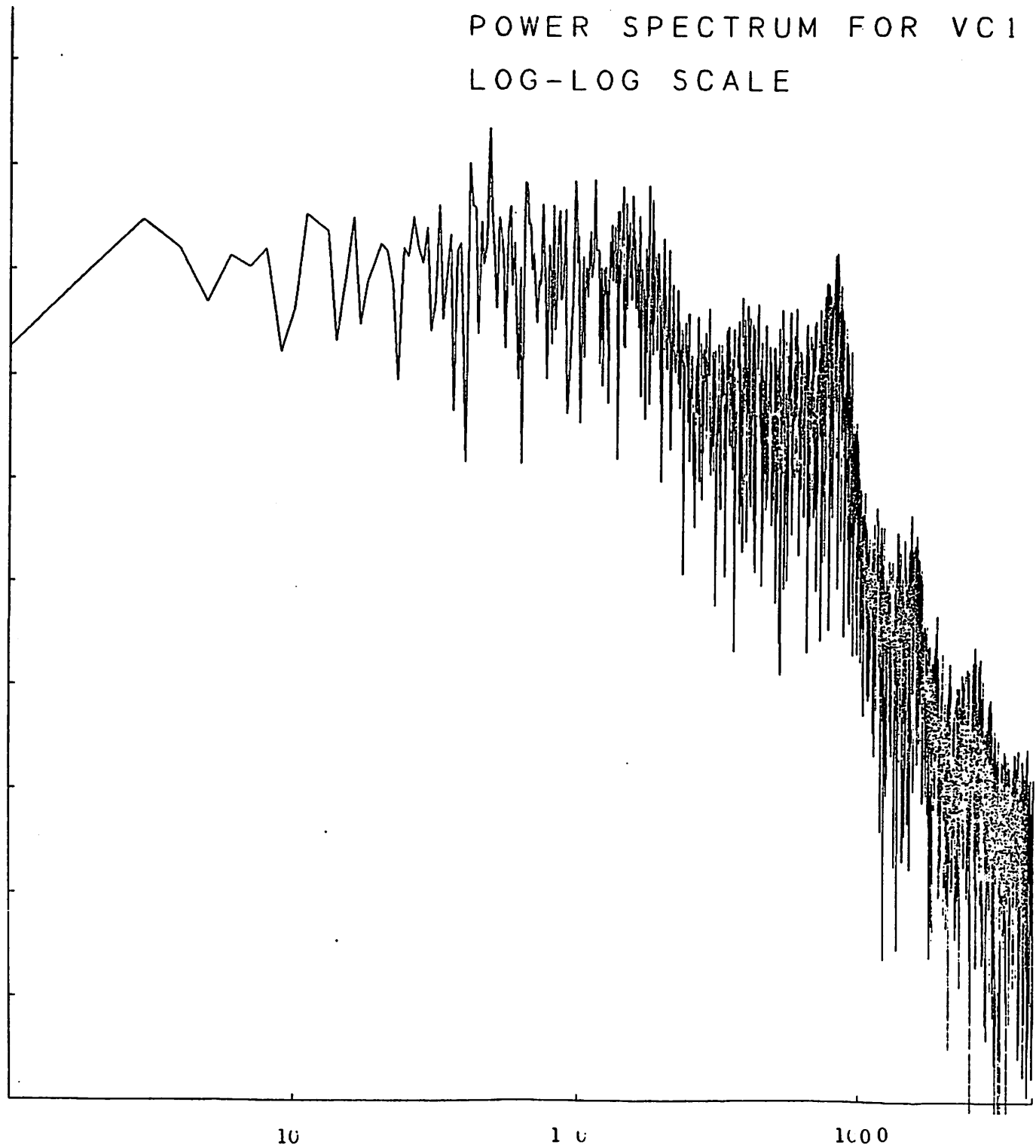


Fig. 16(a)

POWER SPECTRUM FOR VC2
LOG-LOG SCALE

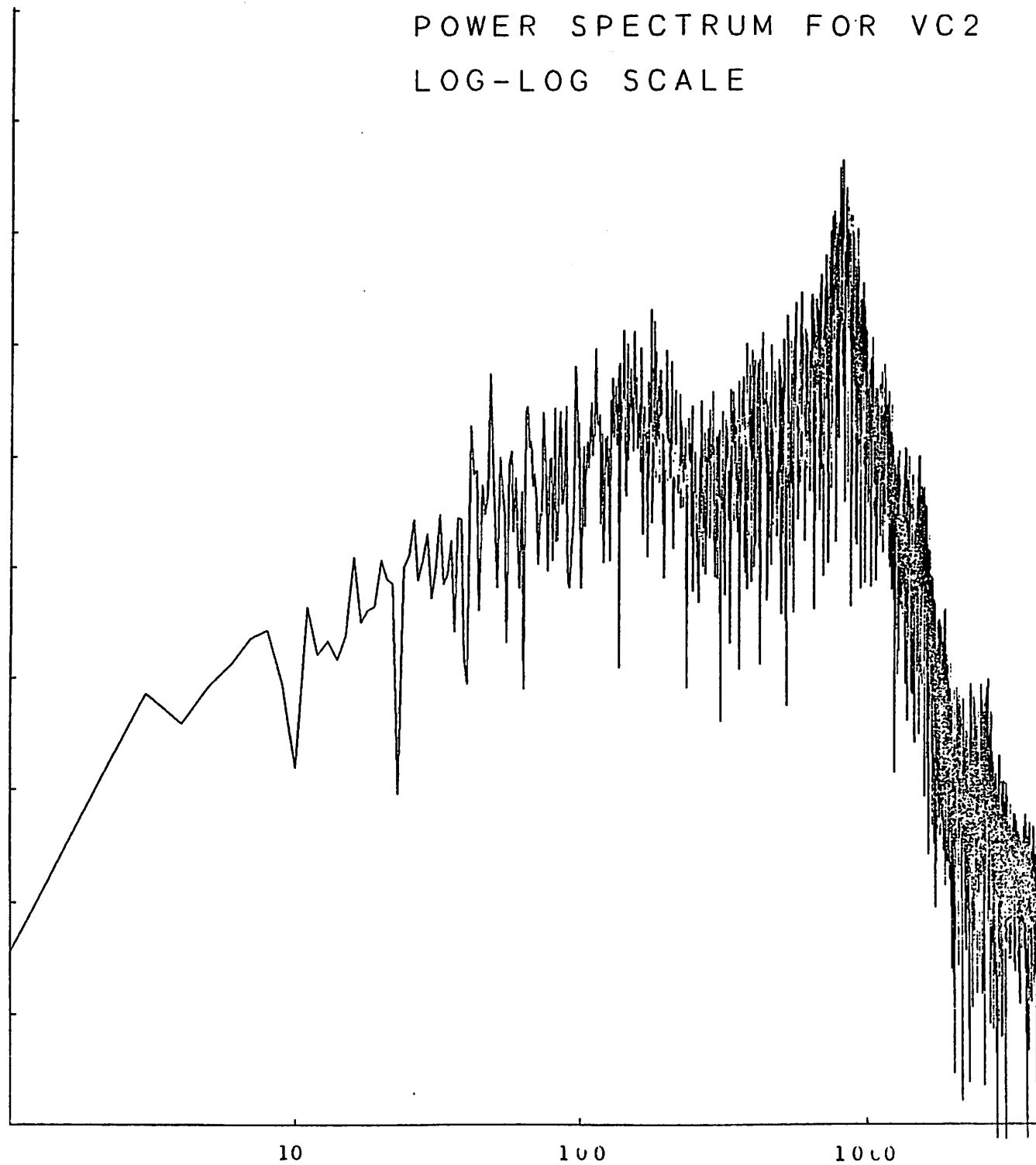


Fig. 16(b)

POWER SPECTRUM FOR IL
LOG-LOG SCALE

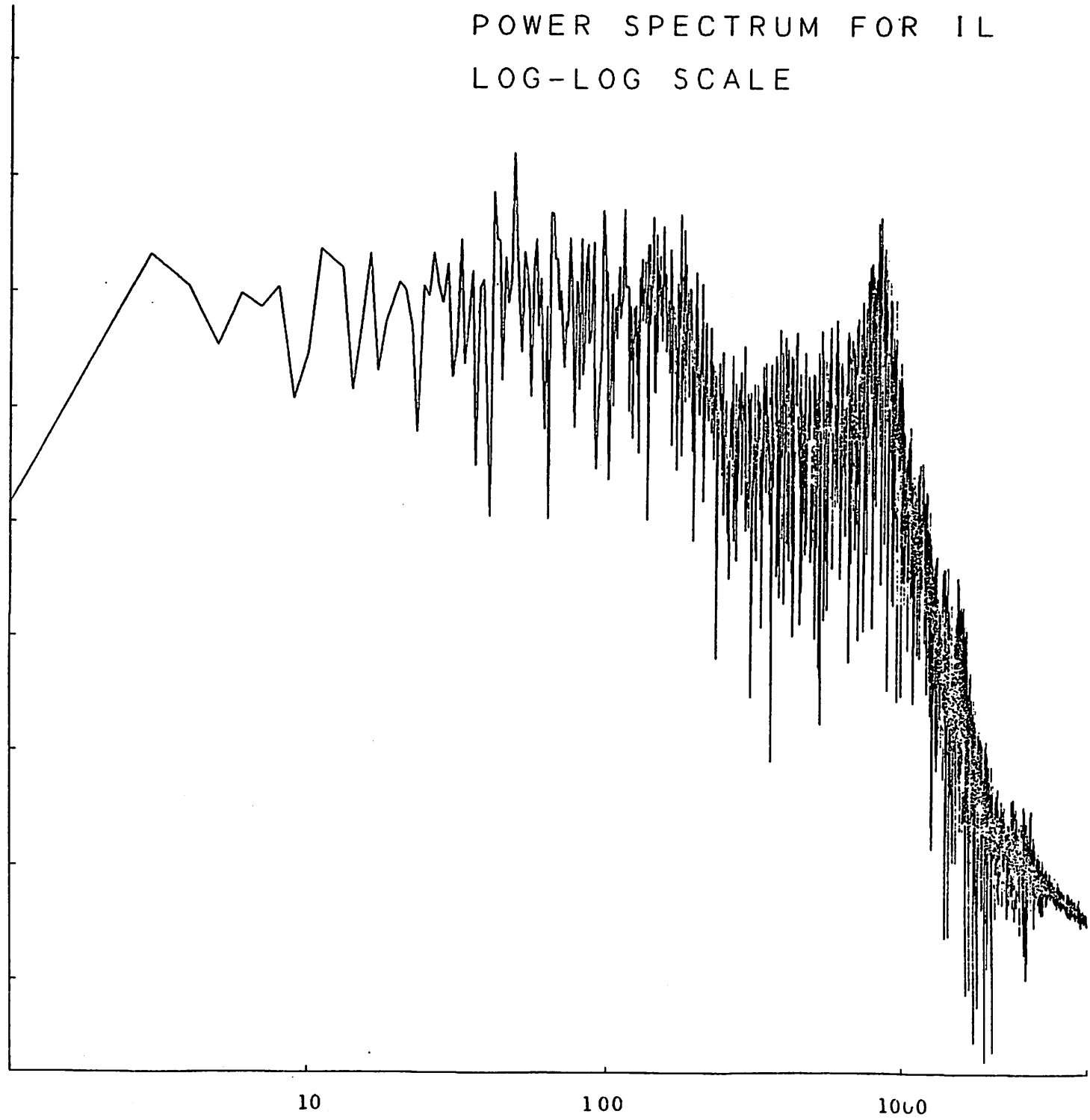
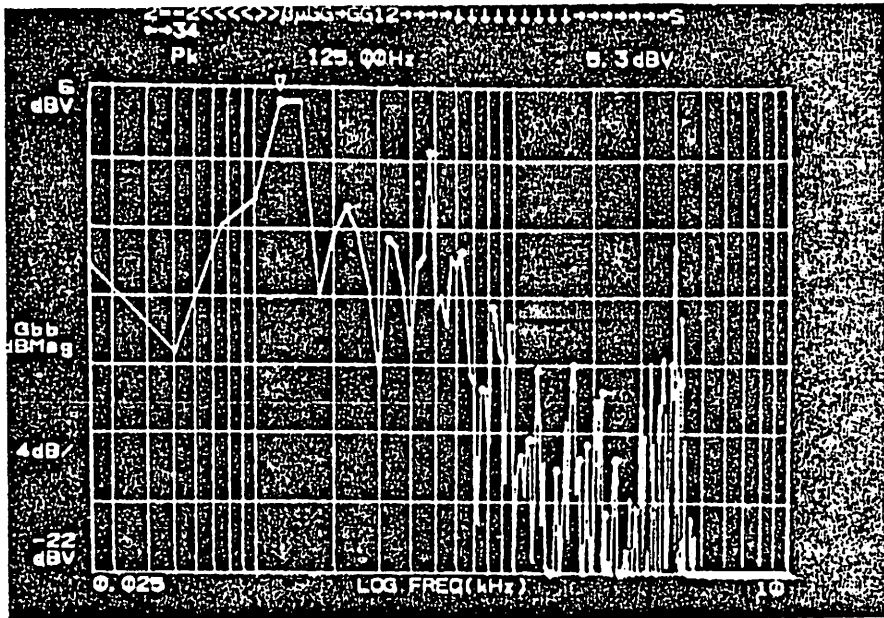
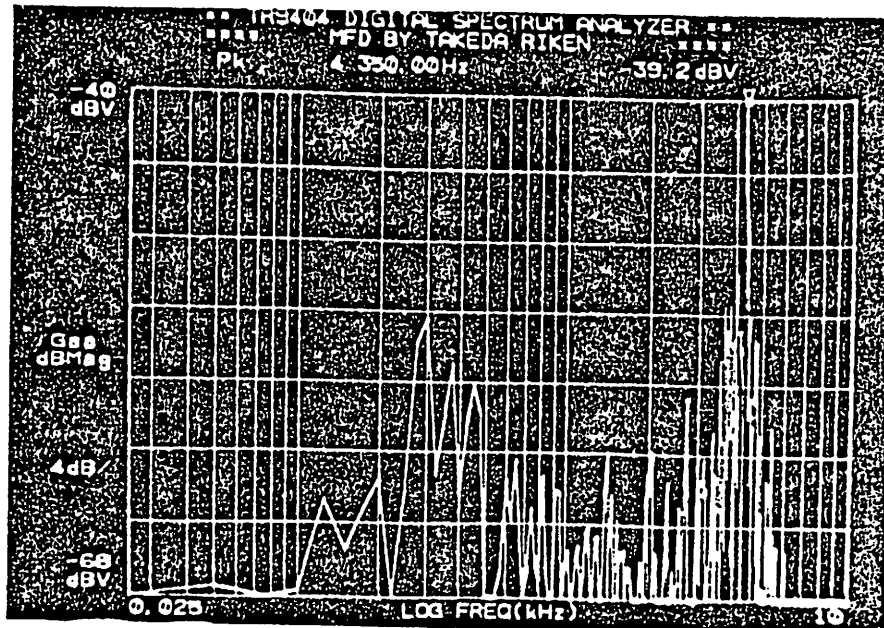


Fig. 16(c)



(a)



(b)

Fig. 17

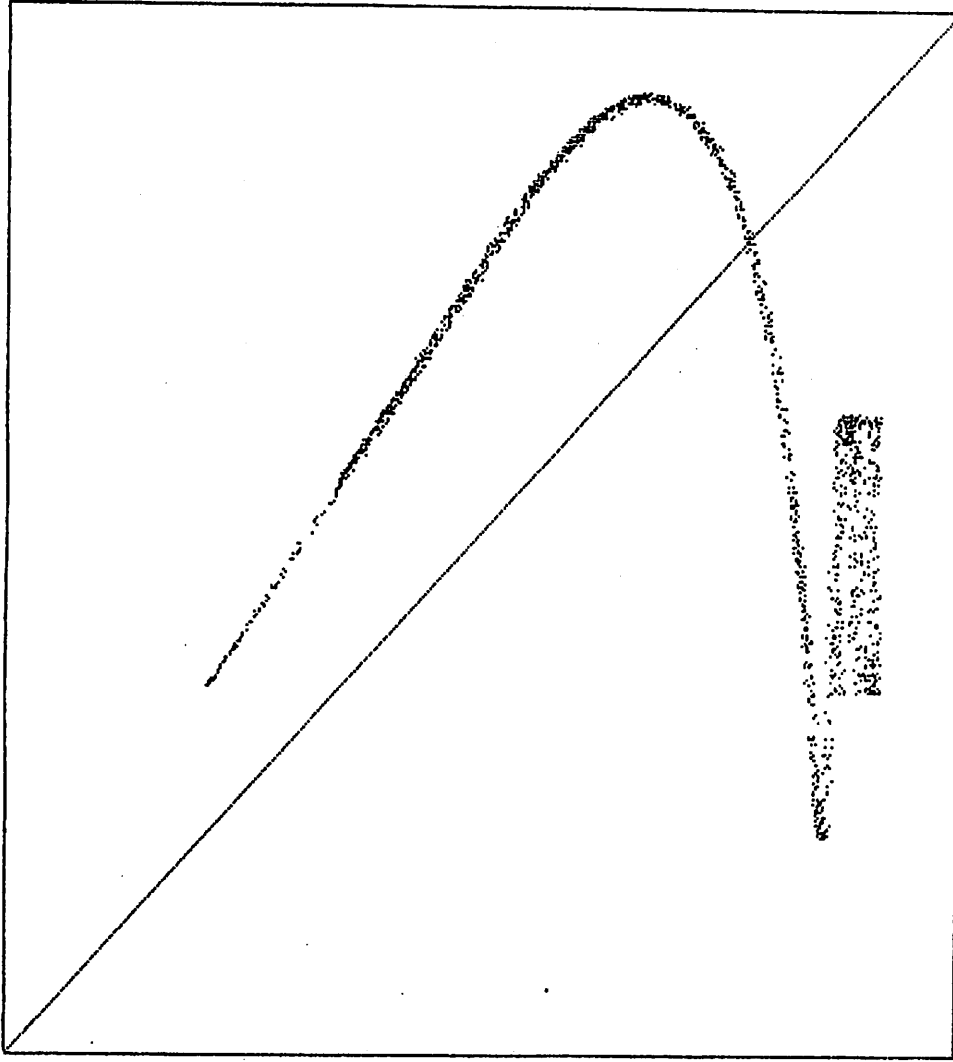


Fig. 18